WATER FOR A HEALTHY COUNTRY FLAGSHIP
www.csiro.au

# Geochemical baseline monitoring: quartz-helium trial

## Final Report

Stanley D Smith
22 March 2015

GISERA Gas Industry Social & Environmental Research Alliance

ISBN (online) 978-1-4863-0583-4

## Citation

Smith SD (2015) Geochemical baseline monitoring: quartz-helium trial. Final Report. CSIRO, Australia.

## Copyright and disclaimer



## Important disclaimer

# Contents

# Figures

# Tables

# Acknowledgments

This report was funded by the Gas Industry Social and Environmental Research Alliance (GISERA). GISERA is a collaborative vehicle established to undertake publicly-reported independent research addressing the socio-economic and environmental impacts of Australia's natural gas industries. The governance structure for GISERA is designed to provide for and protect research independence and transparency of funded research. See www.gisera.org.au for more information about GISERA's governance structure, funded projects, and research findings.

# Executive summary

The estimation of permeability is essential for groundwater modellers and ultimately policy makers, because the amount of leakage, in or out of an aquifer or reservoir, is strongly dependent on this parameter. Furthermore, the permeability of geological materials can vary by many orders of magnitude.

In the Surat Basin, there is a concern about inter-aquifer leakage brought on by the dewatering of coal seams for the extraction of natural gas. In this study, we attempted to determine formation-scale vertical permeabilities in low permeability formations within the Surat Basin. To achieve this, we used a relatively new method where quartz is separated from core samples and the helium contained within the quartz grains is quantified to determine concentrations of helium dissolved within the pore water. These concentrations were fit to solute transport models to ultimately determine the fluid velocity and formation-scale permeability. The advantage of this approach is that permeability is estimated from archived cores (which are relatively easy to obtain) rather than from aquitard pore water (which is very difficult to collect).

Key findings of this report include:

- Diffusion rate measurements suggest that helium results are representative of the past 2-20,000 years
- Monte Carlo simulations of solute transport (constrained by quartz-helium concentrations) within the Evergreen Formation at the Condabri site suggest a fluid velocity of 0.31±0.06mm/year
- Quartz-helium results generally agree with direct dissolved helium measurements (where available), suggesting that the system has been in (quasi) steady state, long enough that helium has equilibrated between the quartz and pore water
- The method appears to be effective in deeper (hotter) sites, but may be unreliable at more shallow (cooler) sites because of the additional time required for helium to reach equilibrium between pore water and quartz

Shortcomings of the method include uncertainties and scatter in the data which in some cases makes interpretation difficult. The uncertainty in fluid velocity may be underestimated because scenarios with transient boundary conditions were not considered – this omission could greatly affect the fluid velocities and vertical hydraulic conductivities presented here. This method is constrained to one-dimensional estimates and without more spatial data, two- and three-dimensional parameter estimates cannot be determined. However, the quartz-helium method can provide estimates formation-scale of vertical permeability in aquitards, where little data currently exist.

# 1 Introduction

The permeability of aquitards is an essential parameter when considering the risk, suitability, and impact of any subsurface project where the isolation of aquifers is necessary. In the Surat Basin, water pressure is decreased in the coal measures for the purpose of desorbing natural gas from coal. Significant changes in pressure have the potential to increase cross-formational flow of groundwater. This could have drawdown impacts on adjacent formations, where the water rights of other users could be affected. To predict the degree of impact, numerical groundwater modelling is required and the correct aquitard permeabilities need to be known. However, the permeability of very low permeability rocks, such as shales, is difficult to assess using traditional techniques and measurements may only be representative at the point of measurement, while not being representative of the entire low permeability sequence. Because fractures and heterogeneity of lithology can greatly increase the permeability as compared to point measurements, there is a need for innovative methods to determine the formation-scale bulk permeability. Currently, there is a lack of vertical permeability data in the Surat Basin. Helium is one tracer that may be strategically used to help constrain permeability. Helium is a noble gas that is completely inert and has a high diffusion rate due to its small mass and inert properties. Helium has a low concentration in the atmosphere and is sparingly soluble in water, resulting in a very low concentration in surface water and groundwater in contact with the atmosphere. However, the subsurface production of helium caused by the radiogenic decay of uranium ($^{235}U$, $^{238}U$) and thorium ($^{232}Th$) can result in helium concentrations that exceed the atmospheric solubility by several orders of magnitude. Because of helium's high diffusivity, it can readily diffuse through low permeability formations and become a tracer for fluid transport rates. In essence, the spatial distribution of helium across a low permeability formation is indicative of the rate of fluid movement, or lack thereof.

Traditional methods to measure helium dissolved in groundwater have relied on collecting water without the loss of any dissolved gases; or alternatively to collect only the dissolved gases using specialized passive headspace samplers. These two methods are effective, but multilevel vertical sampling requires monitoring wells with short screen intervals. Furthermore, these methods yield flow-weighted results, where the most permeable section of a production zone of a well provides the majority of the sample, but the low permeability zones are represented little if at all. Furthermore, if a well yields no water and cannot be purged, it is not possible to collect a noble gas sample using these traditional methods.

An alternative method exists where freshly drill core material is sealed in high-vacuum canisters, preserving the dissolved gases for later analysis in the laboratory. This method has the advantage that samples can be collected from very low permeability formations and at very discreet (0.05 m) intervals. Disadvantages include the need to core new wells to obtain new samples, to have experienced personnel at the drill site, and the potential for up to 30% of the helium being lost during sample handling (Osenbrück et al., 1998).

Another method relies on using helium contained within quartz as a proxy to helium in groundwater. Quartz is a common mineral found in many sedimentary deposits. Unlike minerals, helium easily diffuses in and out of the quartz grains over geological time scales, allowing equilibrium exchange to occur between the quartz and the surrounding fluid. Given a sufficient amount of time, which is a function of temperature and grain size, quartz can provide discreet pore water helium concentrations through any formation that contains a sufficient quantity of quartz. Furthermore, helium is retained in quartz at room temperature meaning that no specialized core preservation is required. The use of this novel tracer has seen little use, but previous work has shown promising results (Lehmann et al., 2003; Smith, 2012). In this study, drillhole chip and core samples from the Surat Basin are analysed using the quartz-helium method. An attempt is made to construct probability density functions of the permeability of the aquitards that separate the major aquifers. If successful, this work will help constrain groundwater flow models aiming to assess cross-formational flow.

# 2 Samples and location

The Surat Basin is located in eastern Queensland and north-eastern New South Wales (Figure 2.1). The basin is considered a portion of the Great Artesian Basin and, in part, overlies the Bowen Basin. APLNG/Origin Energy provided 99 core samples from the Surat Basin. The study area includes the coal seam gas fields of Reedy Creek, Condabri and Talinga (Figure 2.2 and Figure 2.3). These are APLNG's trial sites for reinjecting coproduced waters. All fields are located in south-eastern Queensland, with the Reedy Creek field being located approximately 70 km northeast of Roma, and the Talinga and Condabri fields being located 30 and 46 km southwest of Chinchilla, respectively (Figure 2.2).

Available core samples from the Reedy Creek trial injection site included three bores providing (1) 17 samples from the Westbourne Formation at Reedy Creek SC1-Wb, (2) three samples from the Springbok Sandstone at RCMB2-S, and (3) 26 cores spanning the Precipice Sandstone, Evergreen Formation, and Hutton Sandstone from the bore Reedy Creek MB3-H. Samples from the Condabri trial injection site include 27 samples spanning the Precipice Sandstone, Evergreen Formation, Hutton Sandstone, and Eurombah Formation. Samples from the Talinga field include three bores: (1) three samples from the Gubberamunda Formation from Talinga MB5-G, (2) six samples from the Westbourne Formation from Talinga SC1-Wb, and (3) two samples from the Springbok Sandstone at Talinga MB7-S. Each core subsample weighed approximately 400 g and came from vertical intervals of approximately 20 m. In Addition, four drill cutting samples from Strathblane were provided; these represent cuttings from 1 m intervals at 324–359 m below ground level (mbgl). Samples from Talinga and Strathblane were not assessed in this study as the aquitards of interest are not present. A list of all samples is provided in Appendix A .

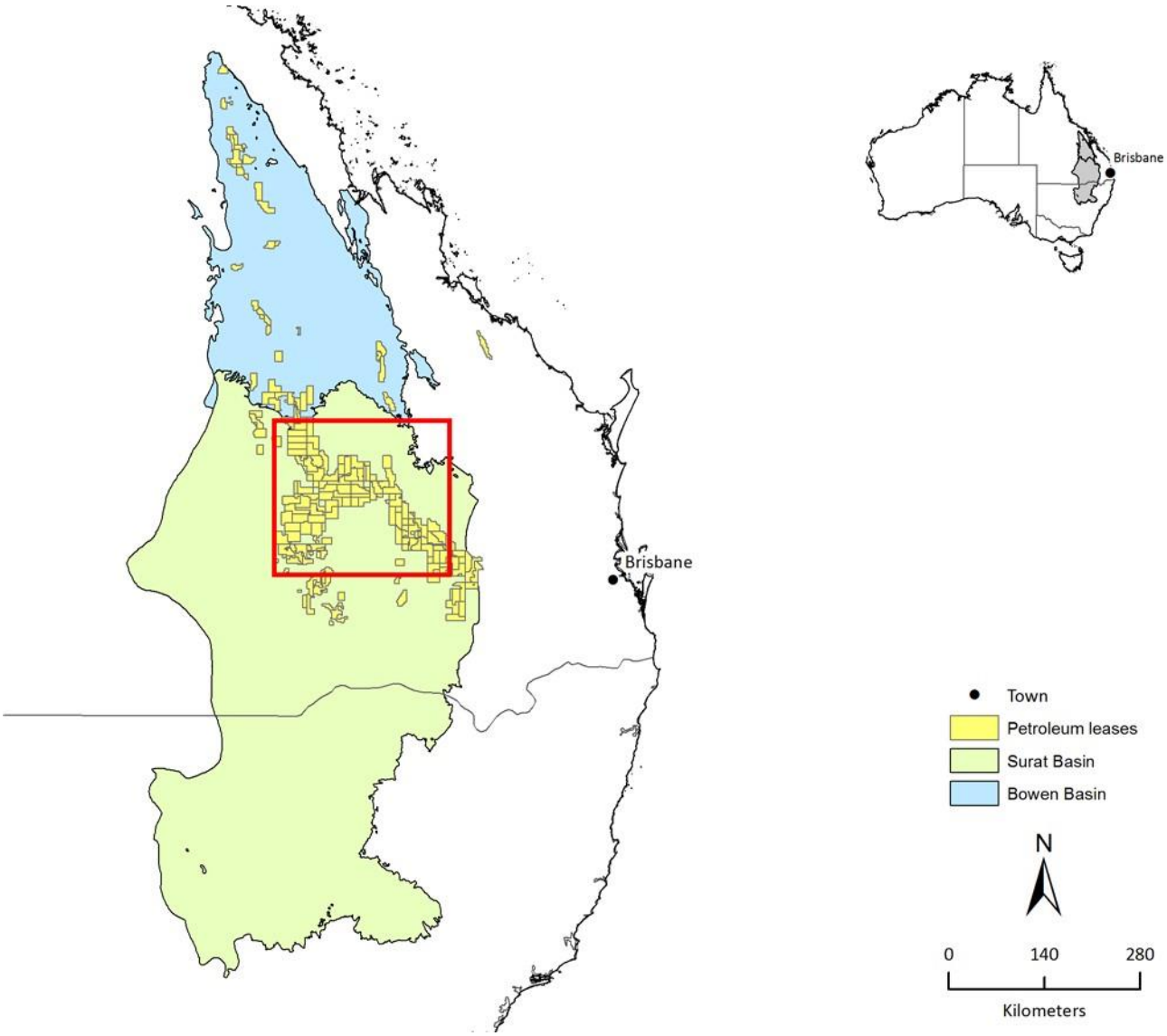


**Figure 2.1 Location of Surat Basin, Bowen Basin, current petroleum leases and the general study area**

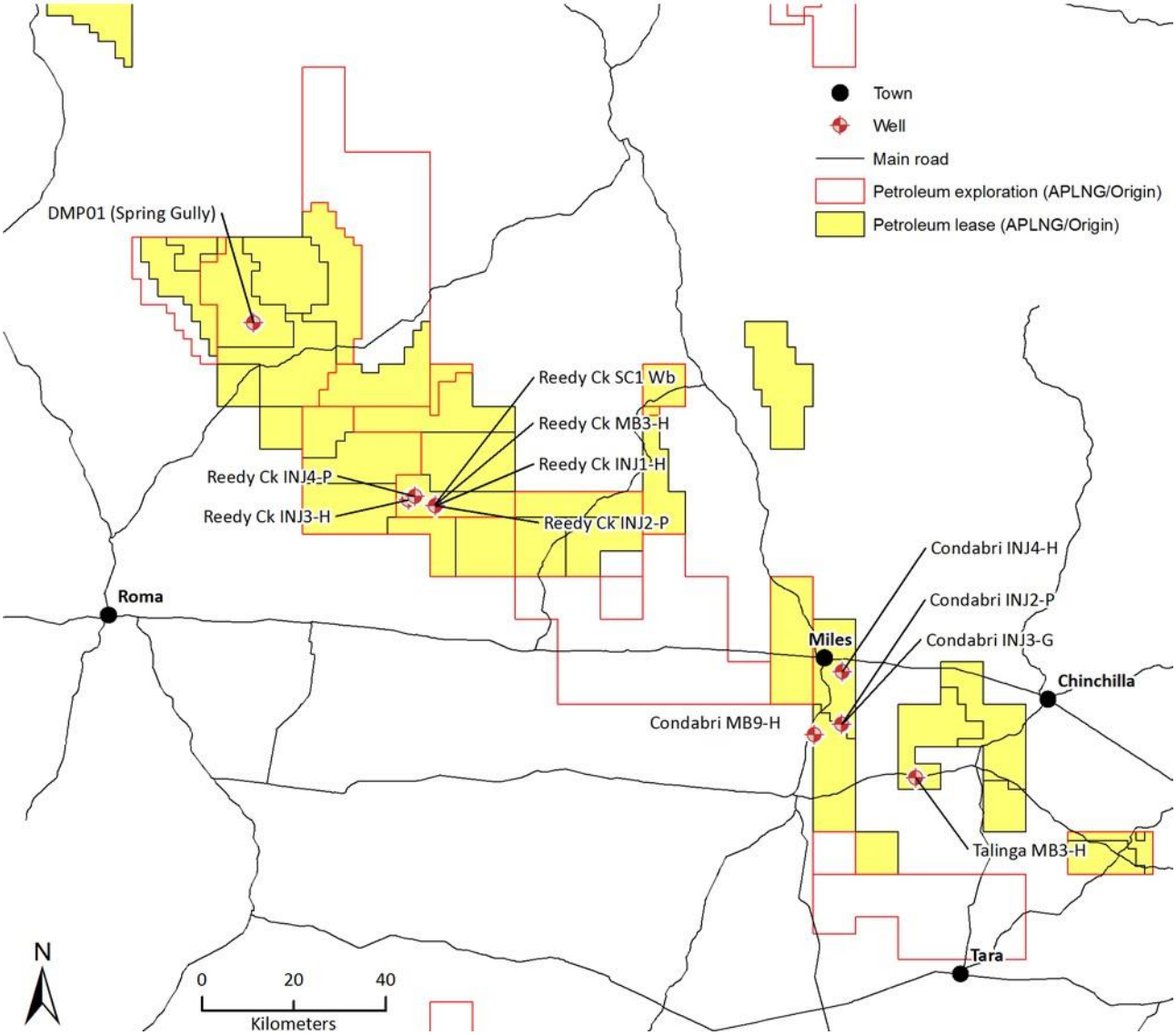


Figure 2.2 Bore locations within the Surat Basin; see

**Figure 2.1 Location of Surat Basin, Bowen Basin, current petroleum leases and the general study area for location of study area**

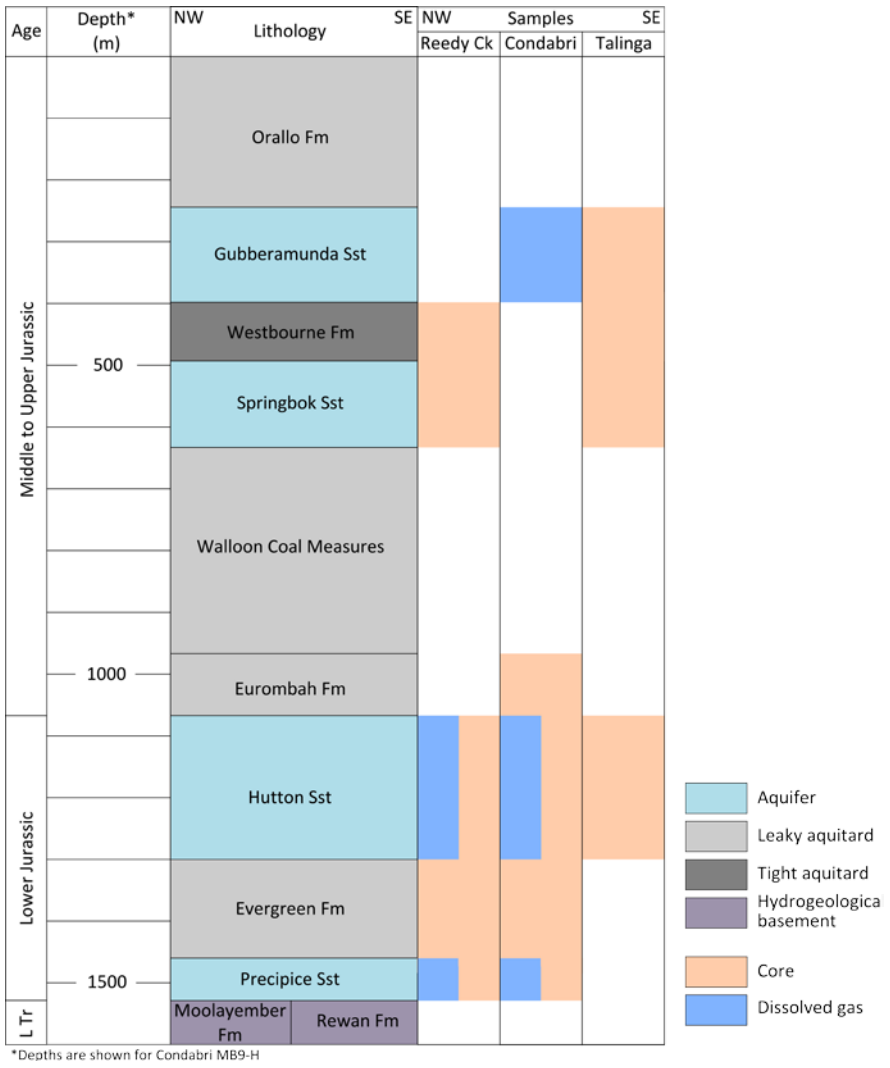


**Figure 2.3 Generalised hydrostratigraphy of the Surat Basin and samples available for noble gas analysis – hydrogeological properties from Smerdon et al. (2012).**

## 2.1 Geology and hydrogeology

The Precipice Sandstone is considered an aquifer unit and was deposited in a braided stream fluvial system and primarily contains quartzose sandstone and fines upwards (Exon, 1976).The lower section is known as the Precipice Braided Sands Formation (BSF). The overlying Evergreen Formation is considered an aquitard and generally contains siltstones, mudstones, and shales; quartzose sandstones can be found in the Boxvale Sandstone member. The Evergreen Formation was deposited in deltaic, fluvial, lacustrine, and marine environments. The Hutton Sandstone conformably overlies the Evergreen Formation; it was deposited in a fluvial environment and generally contains quartzose and immature sandstones. The Hutton Sandstone is considered an aquifer, but low permeability sections are observed (R. Morris, per comm. 27/03/2013). The conformably overlying Eurombah Formation is considered an aquitard and generally contains clay-rich sandstones deposited in swamp and fluvial environments. Samples were not available from the overlying Walloon Coal measures, as the next available samples come from the Springbok Sandstone. The Springbok Sandstone is considered an aquifer and generally consists of sandstones deposited in fluvial, deltaic, swamp and marine environments. Conformably overlying the Springbok Sandstone is the Westbourne Formation, which is considered an unconventional seal due to considerable heterogeneities (University of Southern Queensland, 2011). The formation contains siltstones and mudstones deposited in marine and coastal environments. Conformably overlying in Westbourne Formation is the fluvial deposited Gubberamunda Formation which contains quartzose and lithic sandstones and is considered an aquifer.

X-ray diffraction (XRD) analyses (performed for Origin Energy by Weatherford Laboratories) indicate that quartz is a significant component of all samples. At Reedy Creek within the Hutton and Precipice Sandstones, quartz is dominant (>60%) in 55% of samples and subdominant to co-dominant in the remaining samples. In the analysed samples quartz constitutes a minimum of 26% (Table 2.1). At Condabri, XRD results are similar for the Hutton and Precipice Sandstone. Quartz is dominant in 45% of samples and co-dominant or subdominant in the remaining samples. Furthermore, in these samples, quartz makes up a minimum of 34%.

**Table 2.1 XRD analyses**

| SITE | FORMATION | STATISTIC | QUARTZ (%) | KAOLINITE (%) | ILLITE & ILLITE/SMECTITE (%) | FELDSPAR (ALB) (%) | FELDSPAR (MIC) (%) | CALCITE (%) |
|---|---|---|---|---|---|---|---|---|
| **Reedy CkM B3-H** | Hutton | Mean (σ) | 55.8 (15.8) | 11.8 (4.4) | 15.0 (13.1) | 13.3 (5.4) | 2.8 (2.1) | 0.2 (0.5) |
| | | Min | 25.6 | 5.3 | 4.6 | 7.4 | 0 | 0 |
| | | Max | 74.2 | 21.4 | 43.2 | 28.5 | 5.2 | 2 |
| | Precipice | Mean (σ) | 74.9 (13.2) | 11.6 (5.9) | 4.1 (3.5) | 0.8 (0.7) | 4.3 (2.5) | 2.9 (5.6) |
| | | Min | 61.1 | 3.9 | 1 | 0 | 1.1 | 0 |
| | | Max | 92.7 | 17.1 | 1 | 1.5 | 7.3 | 11.3 |
| **Condabri MB9-H** | Hutton | Mean (σ) | 57.9 (19.2) | 16.9 (8.1) | 6.3 (5.7) | 6.7 (3.3) | 6.2 (3.3) | 5.3 (9.9) |
| | | Min | 34.1 | 4.1 | 0.6 | 1.9 | 0.0 | 0 |
| | | Max | 90 | 33.7 | 17.8 | 15.3 | 9.6 | 26.8 |
| | Precipice | Mean (σ) | 68.0 (28.0) | 16.0 (12.9) | 5.4 (6.0) | 0.3 (0.3) | 2.9 (3.9) | 4.3 (10.1) |
| | | Min | 38.8 | 3.7 | 0 | 0 | 0 | 0 |
| | | Max | 96.3 | 38.1 | 14.8 | 5.2 | 10.1 | 25 |

Source: Origin Energy

## 2.2 Helium production

Helium found in the pore water (and ultimately in quartz) is based on two sources: (1) internal production and (2) external fluxes. While the latter is difficult to approximate without modelling efforts, the internal production rate is readily calculated from uranium and thorium concentrations. Using the isotope ratios and decay constants for these elements and those of the daughter products, the steady state helium production rate (cc STP/$g_r$/year; cubic centimetres gas at standard temperature and pressure per gram rock per year) can be calculated using the equation (Ballentine and Burnard, 2002):

$$^{4}\mathrm{He} = 1.206 \times 10^{-13}[\mathrm{U}] + 2.868 \times 10^{-14}[\mathrm{Th}], \quad (1)$$

where U and Th concentrations are in mg/kg. Beyond the assumption of steady state helium production, it is generally assumed that helium is released into the pore water at the same rate it is produced. The helium production and release rates for two sites in the Surat Basin and the average for the Earth's upper crust are given in (Table 2.2).

## Table 2.2 Formation properties and helium production and release rates

| SITE | FORMATION | n | U (mg/kg) | Th (mg/kg) | POROSITY | BULK DENSITY ($g/cm^3$) | $^4He$ ($10^{-13}$ cc STP/$g_r$/y) | $^4He$ ($10^{-13}$ cc STP/$g_w$/y) |
|---|---|---|---|---|---|---|---|---|
| **Reedy Ck M B3-H** | Hutton Sst | 16 | 5.7 (1.3) | 7.6 (2.8) | 17.3 (4.0) | 2.19 (0.10) | 9.1 (1.8) | 120 (40) |
| | Precipice Sst | 4 | 5.1 (1.1) | 5.0 (1.8) | 16.6 (4.7) | 2.22 (0.13) | 7.5 (1.5) | 100 (40) |
| **Condabri MB9-H** | Hutton Sst | 13 | 3.0 (2.1) | 3.4 (2.0) | 15.0 (5.8) | 2.26 (0.16) | 4.6 (2.5) | 69 (47) |
| | Precipice Sst | 7 | 3.9 (2.2) | 4.7 (3.4) | 11.9 (7.9) | 2.35 (0.23) | 6.1 (2.8) | 120 (100) |
| **Ave Upper Crust*** | | | 2.8 | 10.7 | 8.5 | 2.50 | 6.4 | 190 |
| **Ave Shale**** | | | 6 | 12 | 5 | 2.50 | 10.7 | 534 |

*U and Th concentrations from Ballentine and Burnard (2002), porosity represents average sedimentary rocks (Barrell, 1914 )

**sourced here: http://www.pe.tamu.edu/blasingame/data/z_zCourse_Archive/P663_10B/P663_Schechter_Notes/GR%20Log.PDF calculations in coresummary.xlsx spreadshee t. Values in brackets are standa rd deviations.

# 3 Methods

To determine pore water helium concentrations from helium in quartz, the quartz needs to be separated from the other minerals present in the core. The quartz is then heated to release the helium to allow analysis. To convert the quartz-helium concentration to the equivalent pore water helium concentration, a partitioning factor (helium-accessible volume) is determined by impregnating the quartz with pure helium before it is heated to release that helium before being reanalysed.

## 3.1 Mineral separation

The mineral separation process was the same for all samples with the exception of samples with poor purity of quartz, in which case further processing was necessary and will be described further below. Core samples were roughly disaggregated into pieces with dimensions 30 mm or less using a steel mortar and pestle. Approximately 200 g of the disaggregated sample was first crushed to 10 mm and then to 2 mm using a jaw crusher. The crushed sample was sieved at 1.2 mm after each pass in order to minimize the breakage of quartz grains already disaggregated. The crushed sample was then sieved at 1180, 150, and 53 µm. The >1180 µm fraction was further disaggregated using a porcelain mortar and pestle until the majority of the sample passed through the 150 µm sieve. The >150 µm fraction was further disaggregated and resieved. After the coarser fraction had been sufficiently disaggregated, processing continued with the 54–150 µm fraction (20–40 g). The 54–150 µm fraction was wet sieved for the purpose of removing the clay particles from the mineral grains. The sample was then dried at 50 °C for up to 30 minutes. At this low temperature, no helium loss is expected.

Throughout the mineral separation process, care was taken to only disaggregate the sediment and avoid breaking the quartz. If the helium in quartz grains and pore water was in complete equilibrium, this breakage would not matter. However, equilibrium is less likely in larger grains (>150 µm) so the breakage of larger grains would result in grains with dis-equilibrium ending up in the 54–150 µm fraction. While the samples were carefully processed, there remains a small risk that quartz grains could have been broken and contributed to non-equilibrium helium concentrations – this has not been accounted for in this study.

The dry sample was then magnetically separated using a Frantz isodynamic separator. Minerals with very small magnetic susceptibilities, such as quartz, are separated from minerals with higher magnetic susceptibilities, such as magnetite, pyroxenes, etc. (Rosenblum, 1958). However, this method will not remove fluorite, calcite, feldspar, and some apatite and zircon (Rosenblum, 1958). Separation of muscovite was also marginal in selected samples. Some of these minerals will be removed in later steps, while others are difficult to separate. There is a concern that apatite could release trapped helium in amounts that would overwhelm the amount of helium released from quartz. However, this issue has not occurred in previous work (Smith, 2012).The nonmagnetic sample was then treated with 10% nitric acid for five minutes to remove carbonates, like calcite. If the sample continued to appear unclean, the sample was treated with 2% hydrofluoric acid for an additional five minutes to remove clays and other minerals attached to the quartz grain surfaces. If the sample still contained organic material (likely coal) and/or muscovite, these materials were removed by simple flotation in water (Kowalczuk and Drzymala, 2012). The samples were then oven dried at 50 °C for approximately 10 minutes. The total time necessary to dry the samples should not release measureable amounts of helium. Using an analytical time-dependent solution to the diffusion equation (Crank, 1975), and assuming spherical grains with diameters of 54 µm (the minimum size), less than 0.1% of the helium is released at 50 °C in 1 hour. To release 1% of the helium at this temperature takes approximately 100 days.

## 3.2 Helium release, analysis, and impregnation

Throughout the mineral separation, helium remains trapped within the quartz. To analyse the helium, it must be released from the quartz. For each sample, approximately 2 g of quartz was weighed and put into a custom copper sampler. A custom manufactured stainless steel frit was inserted to prevent loss of sample during subsequent processing. The air and any residual water was removed from the sampler's headspace using a turbomolecular vacuum pump. The sample was then sealed and heated to 290 °C for 5 days. During heating, helium is released into the sampler headspace until a new equilibrium is achieved. As a result, a small, but insignificant, amount of helium remains within the quartz and cannot be measured. Previous work (Smith, 2012) indicates that the residual helium is much less than 1% of the total helium.

The released helium was inlet into a computer controlled all-metal vacuum line with the specific purpose of measuring noble gases in water and gas. Water vapour was removed from the raw sample before it was split into two aliquots. The first aliquot was analysed for $CO_2$, $O_2$, $CH_4$, and $N_2$ using a residual gas analyser quadrupole (Stanford Research Systems RGA 200). Reactive gases were removed from the remaining aliquot using Zr-V-Fe getter material at 280 °C and then split again. One aliquot was further cleaned using charcoal at -196 °C before $^{4}He$, $^{20}Ne$, and $^{22}Ne$ are simultaneously measured using the same quadrupole.
The other aliquot was expanded and split to an acceptably low pressure before $^{36}Ar$ and $^{40}Ar$ were analysed. While no gases aside from helium are expected to be released, it is important to measure the other gases to determine if helium from the atmosphere leaked into the sampler (see below).

By comparing the measured signal of each gas to a reference standard gas (of atmospheric composition) that is analysed before and after every 2–3 samples, a helium concentration is calculated for each sample. Corrections to the helium concentration for atmospheric leakage were necessary for several samples. Because neon is not expected to be released from the sample, any measurable amount of neon can be attributed to atmospheric leakage. The correction goes as:

$$^{4}\mathrm{He}_q = {}^{4}\mathrm{He}_m - {}^{20}\mathrm{Ne}_m \left(\frac{^{4}\mathrm{He}}{^{20}\mathrm{Ne}}\right)_{atm}, \quad (2)$$

where $^{4}\mathrm{He}_q$ is the helium attributed to quartz, $^{4}\mathrm{He}_m$ is the total helium measured, and $\left(\frac{^{4}\mathrm{He}}{^{20}\mathrm{Ne}}\right)_{atm}$ is the atmospheric $^{4}\mathrm{He}/^{20}\mathrm{Ne}$ ratio (0.318). Samples with leakage of up to 5% were considered reliable, whereas samples with greater amounts of leakage were reanalysed (using a new subsample). The average leakage was approximately 0.5% with one outlier at 70%.

The concentration of helium in quartz cannot be directly related to the pore water helium concentration. As such, a partitioning factor must be used. Due to variations in quartz crystal imperfections like fluid inclusions, this partitioning factor varies between samples. To calculate this partitioning factor, known as the helium-accessible volume (HAV; Lehmann et al., 2003), each sample was impregnated with pure helium at 290 °C at a known pressure (400–500 Pa). After the impregnation phase, each sample was heated to release the trapped helium, which was then analysed as above.

The helium-accessible volume, *HAV* (cc He/$cc_{quartz}$), is found using the ideal gas law and normalizing the impregnation results to the experimental temperature and pressure (Lehmann et al., 2003):

$$HAV = \mathrm{He}_{imp} \left(p_1 / p_{imp}\right)\left(T_{imp} / T_1\right), \quad (3)$$

where $He_{imp}$ is the helium concentration in quartz (cc STP He/$cm^3_{quartz}$) at the standard pressure $p_1$ (101,325 Pascal) and standard temperature $T_1$ (273 K). $T_{imp}$ and $p_{imp}$ are the experimental temperature (563 K) and impregnation pressure, respectively.

The helium pore water concentration ($He_w$) can then be calculated using (Lehmann et al., 2003):

$$\mathrm{He}_w = S \times p_1 (\mathrm{He}_{ini} / HAV)(T_{ini} / T_1), \quad (4)$$

where S is the air-water solubility of helium (cc STP He/g atm) while $T_{ini}$ (K) and $He_{ini}$ are the in situ formation temperature and the initial helium concentration measured in the quartz, respectively. In essence, Eq. 3 uses the ideal gas law to calculate the partial pressure of helium in quartz and then converts that value to a pore water helium concentration by means of the solubility. The solubility is dependent on water temperature and salinity and can be calculated using the relation of Weiss (1971) provided the temperature is 0 to 40 °C. Using a geothermal gradient of 28 °C/km and a mean annual surface temperature of 20 °C, analysed samples were at temperatures between 43 and 62 °C. Another relation (Smith and Kennedy, 1983) is valid for temperatures between 0 °C and the critical point of water. This relationship was used for all samples regardless if the temperature was above or below 40 °C. At the environmental temperatures of this study, solubility varies by 5% which is not excessive, but is included for accuracy. The effects of salinity on solubility have not been considered in these calculations. Because salinity decreases the solubility of helium, the pore water helium concentrations can be considered a maximum value. As the temperature increases, the solubility of helium in water decreases until a minimum at 35.5 °C (approximate depth of 550 m) before increasing. A lower solubility works to drive more helium into fluid inclusions within the quartz.

To test if the system is at equilibrium, a quartz sample was split into coarse and fine subsamples. If the system is not in equilibrium, the calculated pore water helium concentrations will not match. A higher helium concentration in the coarse sample would be indicative of higher helium concentrations which have been replaced with lower concentrations. Alternatively, this scenario could be indicative of helium loss in the finer sample during processing. If the helium concentration is higher in the finer sample, the only logical explanation is that the helium concentration has not reached equilibrium with the quartz. A single sample from Reedy Creek MB3-H 1139 m was split into a 54–75 µm fraction and a 75–150 µm fraction and analysed like any other sample.

## 3.3 Diffusivity testing

While the diffusivity of helium has been measured in quartz with fluid inclusions (Gannibal, 2012; Lehmann et al., 2003; Trull et al., 1991) and inclusion-free quartz (Shuster and Farley, 2005), the values have been shown to vary by greater than two orders of magnitude. This uncertainty can translate to the uncertainty regarding equilibration time between quartz and pore water. It is possible that all samples will exhibit different diffusivities; however it is not practical to determine the temperature dependent diffusivity of quartz for every sample as this involves multiple time-steps and analyses for every sample at a range of temperatures. In order to constrain the equilibrium time, the diffusion rate was measured in one sample from within the Precipice Sandstone at 1320 m depth at Reedy Creek bore MB3-H. The sample was chosen as the core contained clean quartz. Like all other samples, the core was crushed, sieved, and further treated to remove impurities. The sample was then impregnated at a high pressure near 1 atm of helium at 290 °C for 30 days to ensure equilibrium of helium was established between the quartz and sampler headspace. The quartz was then sieved to 106–150 µm before being pumped to high-vacuum, as described above, and then sealed in an all-metal sampler. The sample was heated to 290 °C for time steps ranging from 6 to 1321 minutes for a total time of approximately 1900 minutes. After eachtime step, the released helium was analysed as described above and the sampler was resealed online.

The best fit of diffusivity at 290°C ($D_q$) was calculated in an analytical model and assuming spherical geometry (Crank, 1975). Because a single value cannot be given to the grain diameter, diffusivity is often presented as $D_q/a^2$, where $a$ is the radius. An Arrhenius type equation was then used to calculate the maximum diffusivity $D_{0,q}$:

$$D_q = D_{0,q} e^{-E_a/RT}, \quad (5)$$

where $E_a$ is the activation energy determined by Trull et al. (1991; 105 kJ/mol) and R is the gas constant (8.314 J/mol K).

## 3.4 Noble gas direct groundwater sampling

Origin Energy have collected dissolved gas samples using the passive head space diffusion sampler method (Gardner and Solomon, 2009). In summary, the method utilizes a gas-filled nickel tube attached to a hollow stainless steel sampler, which is coated in silicone tubing and allows dissolved gases from the pore water to equilibrate with the gas-filled sample volume. The sampler is placed at the bottom of a small tank which is constantly filled with water pumped from the bore. After 24 hours equilibration, the apparatus is removed from the water and the sample is sealed using a gas tight pinch-off clamp. This method could be questionable as the water flowing past the diffusion cell has been significantly depressurised, which could result in the loss of dissolved gases through dissolution.

At the Condabri field, samples were collected from the Gubberamunda Sandstone (Condabri-INJ3-G; 400 m), Hutton Sandstone (Condabri-INJ4-H; 880 m), and Precipice Sandstone (Condabri-INJ2-P; 1250 m) during a period between October 2012 and February 2013.

At the Reedy Creek field, samples were collected from the Hutton Sandstone (Reedy Ck-INJ1-H and Reedy Ck-INJ3-H; 1025 m) and Precipice Sandstone (Reedy Ck-INJ2-P; 1150 m) during a period between June and August 2012. Additional samples were collected from the Hutton Sandstone (Reedy Ck-INJ3-H; 925 m) Precipice Sandstone (Reedy Ck-INJ4-P; 1256 m) in November 2013.

Samples were also collected at Spring Gully from the Precipice Sandstone (DMP01; 516.5 m). These samples were collected as a time series during April to June 2012.

Samples were analysed at CSIRO Land & Water in Adelaide, SA. The analytical methods are nearly identical to those used to analyse helium in quartz samples. Additional steps are taken to quantify the total dissolved gas pressure.

## 3.5 Modelling methods

### 3.5.1 ONE-DIMENSIONAL STEADY STATE MODEL

#### Fluid velocity

Helium transport modelling was carried out to constrain fluid velocity, and ultimately permeability, using the measured vertical distribution of helium concentrations at each field site. The model used the analytical solution to the advection-diffusion-production equation with constant boundary conditions:

$$C(z) = C_L - \frac{g_w L}{V_z}\left(\frac{1-\exp(zV_z/D_{e,w})}{1-\exp(LV_z/D_{e,w})}\right) + \left(C_U - \frac{g_w L}{V_z}\right)\left(\frac{\exp(zV_z/D_{e,w})-\exp(LV_z/D_{e,w})}{1-\exp(LV_z/D_{e,w})}\right) + \frac{g_w z}{V_z}, \quad (6)$$

where $C(z)$ is the helium concentration at depth $z$, $C_U$ and $C_L$ are the upper and lower helium boundary concentrations, respectively, $g_w$ is the helium release rate into the water, $L$ is the thickness of the formation, $V_z$ is the vertical velocity, and $D_{e,w}$ is the effective diffusivity of helium in water within the formation. The parameters $D_{e,w}$ and $g_w$ are both dependent on effective porosity, $n$:

$$D_{e,w} = D_{0,w} n^m, \quad (7)$$

where $D_{0,w}$ is the free water diffusivity of helium (Jähne et al., 1987) and the exponent term $m$ is an approximation of tortuosity and assumed to equal two (Mazurek et al., 2011). The helium release rate in water is given by:

$$g_w = g_r \rho_r (1/n - 1), \quad (8)$$

where $g_r$ and $\rho_r$ are the helium production rate and density of the rock, respectively. Internal helium production rates were estimated from uranium and thorium concentration from the Hutton and Precipice Sandstones at Condabri MB9-H (Australia Pacific LNG, 2011). From twenty samples with depths from approximately 1050–1550 m, mean concentrations and standard deviations are 3.3±2.1 ppm U and 3.4±2.7 ppm Th. These concentrations give a helium production rate of $5.0\pm3.0\times10^{-13}$ cc STP/$g_{rock}$/year. This is comparable to the production rate of average upper crust of $6.5\times10^{-13}$ cc STP/$g_{rock}$/year (Ballentine and Burnard, 2002). It is assumed that the release rate of helium into the pore water is equal to the production rate. In other words, the helium production-release system is at steady state.

Underlying assumptions of Eq. 6 include that the hydraulic parameters are constant within the model domain and that helium transport is at steady state. Furthermore, it is assumed that horizontal fluid flow and helium transport are insignificant in comparison to vertical helium transport.

The assumption of steady state is used because it is not possible to determine an initial condition for helium in a groundwater system without independent information (Mazurek et al., 2011). Given a thickness of 160 m for the Evergreen formation at Condabri and further assuming a porosity of 0.15 and temperature of 60 °C, the time to reach steady state by diffusion exceeds 1.5 My (assuming two characteristic times to reach steady state) but would be shorter by adding a component of advection. With the current knowledge, it is not possible to know if the basin is at steady state. As such, the assumption remains useful unless the data suggests otherwise.

**Boundary conditions**

To derive Eq. 6, it is assumed that the helium boundary conditions are constant. This assumption is based on an assumption that deep hydrogeological systems, such as the Surat Basin, are relatively static and that helium concentration probably have little fluctuation. The use of a steady state model also comes from a lack of data that would indicate a transient condition and a lack of data to constrain an initial condition. The exclusion of transient scenarios likely has consequences for the modelled fluid velocities

Another aspect of the boundary conditions, which can be assessed here, is the position of the boundary. As the Surat Basin is a heterogeneous system, the depth of the hydrogeological boundary may not be apparent from the geological units. This complication is known for the Hutton Sandstone as it does not always act as an aquifer. Gamma logs were assessed to determine appropriate boundaries for the aquitard that includes the Evergreen Formation. To help interpret the gamma logs, gamma readings were averaged at 10 m intervals and then applied a colour gradient with end members appropriate for clean sand and shale (see figures in Section 4.4 and Appendix B ). Modelling was also done with named geological boundaries allowing a comparison.

## Hydraulic conductivity

Using the modelled fluid velocity, the hydraulic conductivity (*K)* of the formation can be derived using Darcy's Law:

$$q = -K\nabla h, \tag{9}$$

where $\nabla h$ is the vertical hydraulic head gradient and $q$ is the specific discharge. Converting the specific discharge to velocity and rearranging yields:

$$K = -\frac{V_z n}{\nabla h}. \tag{10}$$

## Monte Carlo simulation

Because uncertainty exists in each observation, probability density functions (PDFs) and cumulative distribution functions (CDFs) were determined for $V_z$ and $K$. In a Monte Carlo simulation of 10,000 iterations, all observations were randomly varied and the velocity was chosen that corresponded to the lowest misfit. The helium concentration measurements were given normal distributions with the total

uncertainty being the estimated analytical uncertainty (7%). The uncertainty was increased by factors of two and three to determine the sensitivity to this parameter. The parameter $n$ was varied with a normal distribution based on porosity measurements throughout the Surat Basin (Kellett et al., 2012). The parameter $g_r$ was varied with a linear distribution based on U and Th concentrations measured on core samples from Condabri MB9-H (Australia Pacific LNG, 2011). All of these equations and distributions were written into a code that was run in MATLAB® and produces a text file of results. Before calculating the fit parameters of the PDFs using standard methods of maximum likelihood estimation, statistical outliers were removed.

## Evergreen Formation at Condabri

The fluid velocity and hydraulic conductivity of aquitards at Condabri were modelled using two approaches. The first approach used the stratigraphic boundaries where the Evergreen Formation is bounded by the Precipice and Hutton sandstones. This means that the Evergreen Formation is 160 m thick and the helium boundaries are those measured in the adjacent sandstone formations.

In the second approach, gamma logs were used to indicate where sandy units were located. This approach gives more confidence in the boundaries when units like the Hutton Sandstone are predominantly composed of high gamma (shale and clay rich) sediments that likely act as aquitards instead of aquifers.

For the Monte Carlo simulations, the observations $C_L$, $C_U$, $n$, and $g_r$ were varied within reasonable ranges given in Table 3.1. To determine the hydraulic conductivity, the hydraulic gradient was calculated as the head difference between the Hutton and Precipice sandstones divided by the thickness of the Evergreen Formation and is 0.25 (Australia Pacific LNG, 2013).

**Table 3.1 Input parameters for Monte Carlo simulations of the Evergreen Formation at Condabri (standard case)**

| PARAMETER | SYMBOL | UNITS | MEAN | σ/± | Distribution |
|---|---|---|---|---|---|
| Porosity* | $n$ | - | 0.15 | 0.06 | normal |
| Production | $g_r$ | $10^{-13}$ cc STP/g/y | 5.0 | 3.0 | linear |
| Upper Boundary | $C_U$ | $10^{-6}$ cc STP/g | 8.6 | 0.6 | normal |
| Lower Boundary | $C_L$ | $10^{-6}$ cc STP/g | 19.5 | 1.4 | normal |

*Minimum porosity was fixed at 0.04

## Westbourne Formation at Reedy Creek

The parameters for modelling the Westbourne Formation at Reedy Creek were very similar to the parameters present at the Evergreen Formation at Condabri. Differences are limited to the boundary conditions, helium production rate, and porosity and temperature, which both affect the effective diffusivity of helium. Defining the boundary conditions within the adjacent aquifers was not possible because samples were not collected from these formations. As the next best option, the upper and lower helium measurements within the Westbourne Formation were used as the boundaries. This is a reasonable assumption provided that the system is in steady state (i.e. the helium concentrations in the Westbourne Formation are not a relic of a previous helium distribution).

The helium production rate was initially set to match the Evergreen Formation as no other data exists; however it was found that the production rate needed to be increased substantially (but within geological reason) to match the observed helium profile. Given the sensitivity to this parameter, the uncertainty in this measurement was not considered, as slight variations in production substantially reduced the fit of the model with the observations. The modelling parameters for the Westbourne Formation, including those used in the Monte Carlo simulations, are summarized in Table 3.2.

**Table 3.2 Input parameters for Monte Carlo simulations of the Westbourne Formation at Reedy Creek**

| PARAMETER | SYMBOL | UNITS | MEAN | σ/± | Distribution |
|---|---|---|---|---|---|
| Porosity* | $n$ | - | 0.26 | 0.06 | normal |
| Production | $g_r$ | $10^{-13}$ cc STP/g/y | 50 | 0 | n/a |
| Upper Boundary | $C_U$ | $10^{-6}$ cc STP/g | 2.4 | 0.2 | normal |
| Lower Boundary | $C_L$ | $10^{-6}$ cc STP/g | 4.2 | 0.3 | normal |

*Minimum porosity was fixed at 0.04

## Evergreen Formation at Reedy Creek

The parameters used to model fluid flow through the Evergreen Formation at Reedy Creek were very similar to those used for this formation at Condabri (Table 3.1). However, modelling was only completed with the stratigraphic boundaries as there is no clear Lithological boundary present from the gamma logs.

# 4 Results

## 4.1 Helium diffusivity in quartz

The time-stepped helium release measurements from sample Reedy Creek MB3-H 1320 are given in Figure 4.1. Relatively large error bars are indicated as the amount of helium released in several steps greatly exceeded the amount of helium to which the analytical equipment is calibrated.

The analytical model gives a diffusivity ($D_q/a^2$) of $8.9\times10^{-5}$ 1/s at 290 °C. Using the mean grain size, assuming a linear distribution of grain sizes, $D_{0,q}$ is $1.6\times10^{-3}$ $m^2/s$. This value is significantly greater than the diffusivities determined by previous studies (Gannibal, 2012; Lehmann et al., 2003; Trull et al., 1991). Using this data, equilibration times for 150 µm grains (the largest in this study) is 274,000 years at 20 °C, 18,000 years at 40 °C, and 2,000 years at 60 °C. For the deeper samples in this study (below the Walloon CM), this means pore water helium derived from quartz helium should represent the hydraulic regime over the last 2–20,000 years. At shallower depths, and thus cooler temperatures, this implies the equilibration time could be much longer and presents a greater uncertainty regarding whether there is equilibrium of helium between quartz and pore water.

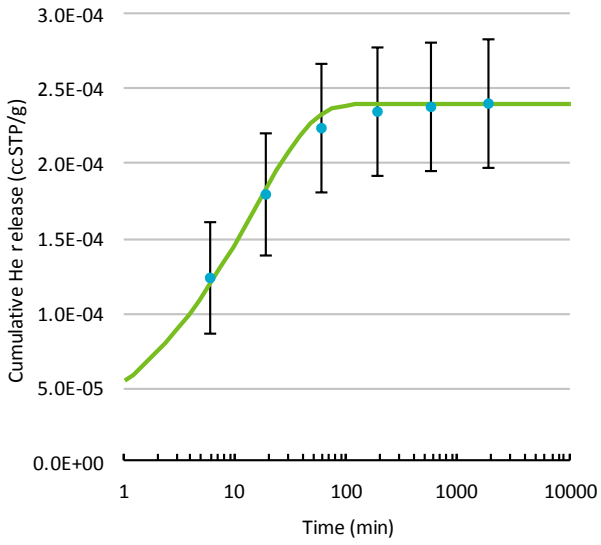


**Figure 4.1 Helium release in quartz from Reedy Creek MB3-H 1320 m. Curved line is the best fit modelled result**

## 4.2 Helium concentrations in quartz

Helium concentrations in quartz are given in and Table 4.1 and Table 4.2.

### 4.2.1 CONDABRI

At Condabri MB9-H the helium concentrations in quartz range from $0.8–1.7\times10^{-6}$ cc STP/$cm^3$ – a factor of 2.2. Helium concentrations in quartz have no strong trends with depth, but helium tends to decrease going down through the Hutton Sandstone before increasing slightly and being somewhat scattered in the Evergreen Formation and Precipice Sandstone (Table 4.1).

**Table 4.1 Quartz-helium results for Condabri MB9-H**

| FORMATION | DEPTH (m) | $^4He_{qua\ rtz}$ ($10^{-6}$ cc STP/cm$^3$) | HAV ($10^{-3}$ cc/cm$^3$) | $^4He_{wat\ er}$ ($10^{-5}$ cc STP/g) |
|---|---|---|---|---|
| **Eurombah Formation** | 1041 | 1.31 | 1.52 | 0.878 |
| | 1061 | 1.55 | 1.09 | 1.46 |
| **Hutton Sandstone** | 1152 | 1.14 | 1.52 | 0.781 |
| | 1214 | 0.881 | 1.32 | 0.703 |
| **Evergreen Formation** | 1271 | 0.785 | 0.969 | 0.860 |
| | 1360 | 1.33 | 1.34 | 1.07 |
| | 1400 | 0.879 | 1.30 | 0.736 |
| | 1420 | 1.14 | 1.02 | 1.22 |
| | 1440 | 1.61 | 0.845 | 2.08 |
| **Precipice Sandstone** | 1455 | 1.73 | 1.12 | 1.70 |
| | 1481 | 1.02 | 0.579 | 1.95 |

### 4.2.2 REEDY CREEK

At Reedy Creek SC1-Wb the helium concentrations in quartz ranged from 1.3–8.3×$10^{-7}$ cc STP/cm$^3$, representing a factor of 6.4 (Table 4.2). Helium concentrations in quartz appeared to be low at the boundaries, with a general increase towards the middle of the formation. At Reedy Creek MB3-H the helium concentrations in quartz ranged from 0.6–2.8×$10^{-6}$ cc STP/cm$^3$, representing a factor of 4.5. Helium concentrations in quartz tended to decrease with depth.

**Table 4.2 Quartz-helium results for Reedy Creek MB3-H and Reedy Creek SC1-Wb**

| FORMATION | DEPTH (m) | $^4He_{quartz}$ ($10^{-6}$ cc STP/cm$^3$) | HAV ($10^{-3}$ cc/cm$^3$) | $^4He_{water}$ ($10^{-5}$ cc STP/g) |
|---|---|---|---|---|
| **Westbourne Formation** | 244 | 0.492 | 1.66 | 0.244 |
| | 254 | 0.495 | 1.52 | 0.307 |
| | 267 | 0.833 | 1.10 | 0.713 |
| | 284 | 0.561 | 0.838 | 0.633 |
| | 311 | 0.834 | 0.749 | 0.390 |
| | 319 | 0.789 | 1.19 | 0.631 |
| | 347 | 0.129 | 0.292 | 0.419 |
| **Hutton Sandstone** | 841 | 1.65 | 1.86 | 0.880 |
| | 900 | 2.79 | 1.76 | 1.59 |
| | 960 | 1.54 | 1.12 | 1.39 |
| | 1020 | 0.988 | 0.908 | 1.11 |
| | 1080 | 0.897 | 1.59 | 0.580 |
| | 1139* | 1.33 | 1.16 | 1.19 |
| | 1139** | 1.14 | 1.10 | 1.08 |
| **Evergreen Formation** | 1220 | 0.686 | 1.04 | 0.697 |
| | 1260 | 0.660 | 1.09 | 0.641 |
| | 1280 | 1.35 | 0.884 | 1.63 |
| **Precipice Sandstone** | 1320 | 0.623 | 0.681 | 0.980 |

*53–75 µm; **75–150 µm

## 4.3 Helium-accessible volumes

Helium-accessible volumes at 290 °C are given in Table 4.1 and Table 4.2

### 4.3.1 CONDABRI

The mean helium-accessible volume at Condabri MB9-H is $1.1\pm0.2\times10^{-3}$ cc/cm$^3$ (Table 4.1). There is no clear trend with depth, but some samples with lower initial helium release tend to have higher helium-accessible volumes and vice versa.

### 4.3.2 REEDY CREEK

The mean helium-accessible volumes at Reedy Creek are 9.8±3.9 for SC1-Wb and $1.2\pm0.4\times10^{-3}$ cc/cm$^3$ for MB3-H (Table 4.2). The trend with depth in Reedy Creek MB3-H shows that the helium-accessible volumes decrease with depth, roughly following the trend of helium in quartz concentrations. This contrasts with the trends seen in the Condabri samples. At this point it is unclear what could be causing a given trend aside from depositional factors such as grain size/shape or provenance.

## 4.4 Helium concentrations in pore water

### 4.4.1 CONDABRI

Pore water helium concentrations derived from Eq. 4 are given in Table 4.1. Helium concentrations are $2.0\times10^{-5}$ cc STP/g in the Precipice Sandstone, $0.7–2.1\times10^{-5}$ cc STP/g in the Evergreen Formation with a general decreasing upward trend (Figure 4.2). Concentrations in the Hutton Sandstone are relatively constant at $0.7–0.9\times10^{-5}$ cc STP/g before increasing sharply into the Eurombah Formation at $1.5\times10^{-5}$ cc STP/g.

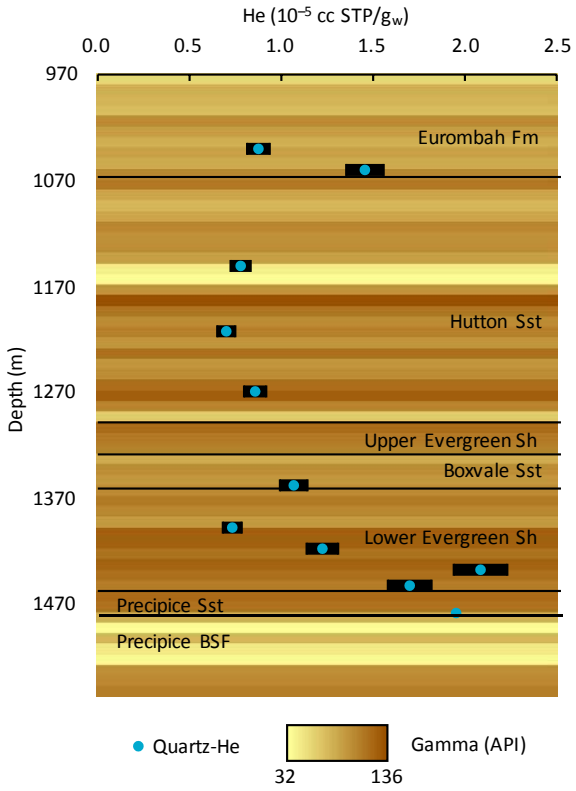


**Figure 4.2 Pore water helium concentrations and 10 m averaged gamma values from Condabri MB9-H**

### 4.4.2 REEDY CREEK

Pore water helium concentrations derived from Eq. 4 are given in Table 4.2. Helium concentrations are $1.0\times10^{-5}$ cc STP/g in the Precipice Sandstone, $0.6–1.1\times10^{-5}$ cc STP/g in the Evergreen Formation with the upper analysis with the higher concentration (Figure 4.3a). Concentrations in the Hutton Sandstone are $0.6–1.6\times10^{-5}$ cc STP/g with an upward increasing trend up to 900 mbgl and then the concentration decreases. Concentrations in the Westbourne Formation are lower than deeper formations at 0.3–0.7 cc STP/g; helium concentrations are generally higher in the centre of the formation as compared to the edges (Figure 4.3b).

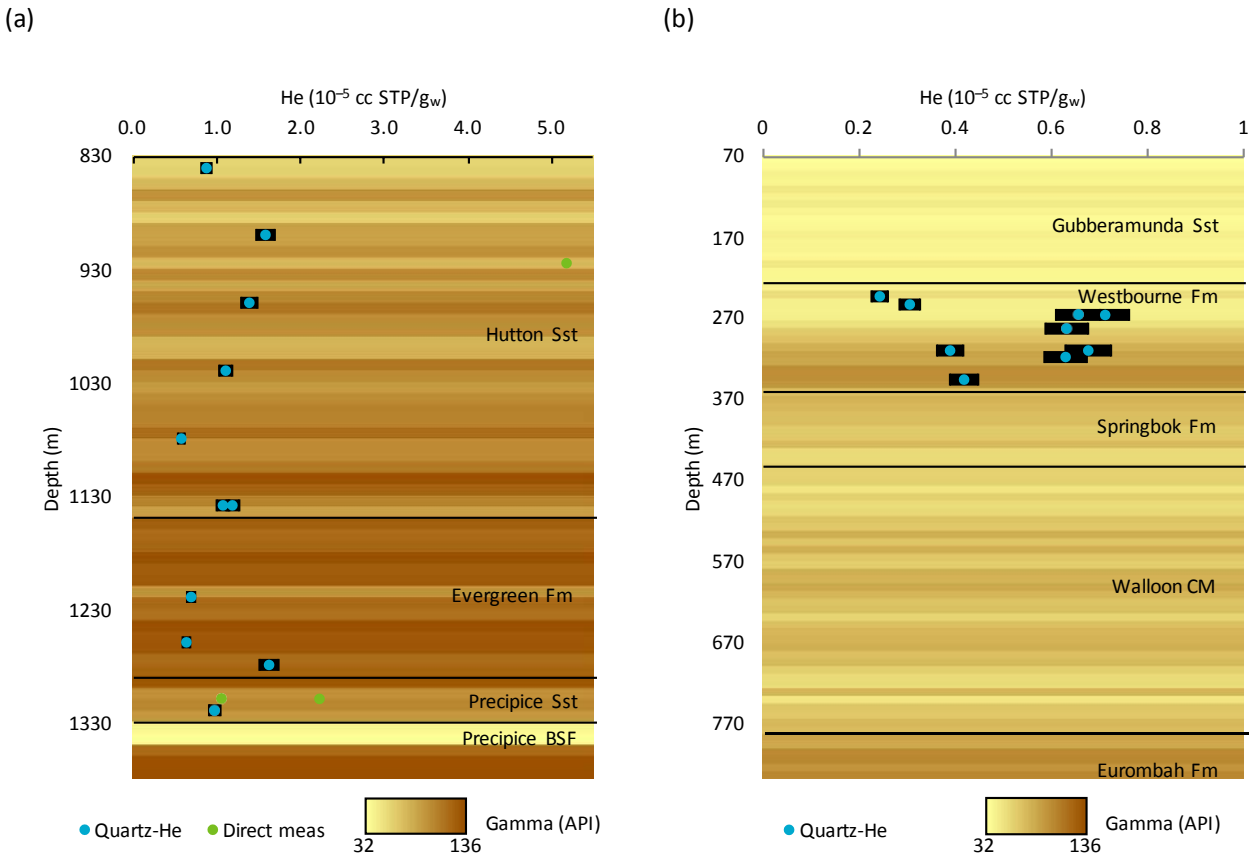


**Figure 4.3 Pore water helium concentrations and 10 m averaged gamma values from (a) Reedy Creek MB3-H and (b) Reedy Creek SC1-Wb**

### 4.4.3 DIRECT MEASUREMENTS

Groundwater helium concentrations are given in Table 4.3. In the Condabri field, only one sample, coming from the Gubberamunda Sandstone, was properly sealed giving a helium concentration of $6\times10^{-5}$ cc STP/g, exceeding atmospheric solubility by over three orders of magnitude.
At the Reedy Creek field, the Precipice Sandstone has helium concentrations of $1–2\times10^{-5}$ cc STP/g, exceeding atmospheric solubility by a factor of approximately 200–400. This range of concentrations is surprising considering that the two sample sites are <5 km apart. The Hutton Sandstone had a higher concentration at $5\times10^{-5}$ cc STP/g. The remaining two samples from the Hutton Sandstone at Reedy Creek have helium concentrations similar to atmospheric solubility; this suggests that the gas leaked from the sample container and has been replaced with gas of atmospheric composition. As such, these two analyses are not reliable for any further discussion.

At the Spring Gully field, the Precipice Sandstone has helium concentrations of approximately $3\times10^{-5}$ cc STP/g. This value is an average of 13 analyses, where one analysis appears atmospheric, while an additional two analyses have helium concentrations that are at least an order of magnitude lower than the average.

**Table 4.3 Direct helium measurements**

| BORE | FORMATION | DEPTH (m) | $^4He$ ($10^{-5}$ cc STP/g) |
|---|---|---|---|
| **Condabri-INJ3-G** | Gubberamunda | 400 | 6.08 |
| **Condabri-INJ4-H*** | Hutton | 880 | - |
| **Condabri-INJ2-P*** | Precipice | 1250 | - |
| **Reedy Ck-INJ1-H**** | Hutton | 1025 | 0.00 |
| **Reedy Ck-INJ3-H**** | Hutton | 1025 | 0.01 |
| **Reedy Ck-INJ3-H** | Hutton | 925 | 5.18 |
| **Reedy Ck-INJ4-P** | Precipice | 1256 | 2.23 |
| **Reedy Ck-INJ2-P** | Precipice | 1150 | 1.06 |
| **DMP01 (Spring Gully)** | Precipice | 516.5 | 2.68±1.95 |

*sample not sealed, no analysis; **leak likely, atmospheric composition

## 4.5 Modelling results

### 4.5.1 CONDABRI

#### Evergreen Formation only

Monte Carlo simulations of one-dimensional helium transport across the Evergreen Formation at Condabri MB9-H yield a PDF of velocity with a logarithmic normal distribution (Figure 4.4a). The mean vertical fluid velocity is $3.1\pm0.6\times10^{-4}$ m/year. The median is $3.1\times10^{-4}$ m/year and the mode is $2.9\times10^{-4}$ m/year. The cumulative probability (Figure 4.4b) indicates a 90% probability that the vertical velocity is less than $3.8\times10^{-4}$ m/s and a 99% probability that the velocity is less than $4.7\times10^{-4}$ m/year. By increasing the uncertainty by a factor of two and three causes the mean to increase by 5 and 15%, respectively. The standard deviations increased by 77 and 181%. The median values increased slightly at 1 and 4% and the mode decreased by 7 and 15%. The 90% probabilities increase by 11 and 22%, and 99% probabilities increase by 29 and 64% (Figure 4.5). Best-fit solutions and 95% probability is given in Figure 4.6. The parameters that control the best-fit velocity are given in Appendix C showing histograms of porosity, diffusivity, and production rate.

The modelled vertical hydraulic conductivity is shown in Figure 4.7. A logarithmic normal distribution fits this data relatively well, but there appears to be an offset, which could be caused by outliers or some bias in the data fitting. The mean value is $6.1\pm2.6\times10^{-12}$ m/s with a mode of $4.6\times10^{-12}$ m/s. The 90% and 99% probabilities are $7.7\times10^{-12}$ and $12\times10^{-12}$ m/s, respectively. Because the uncertainty of the vertical hydraulic gradient were not considered, it's possible that these values are not the most conservative.

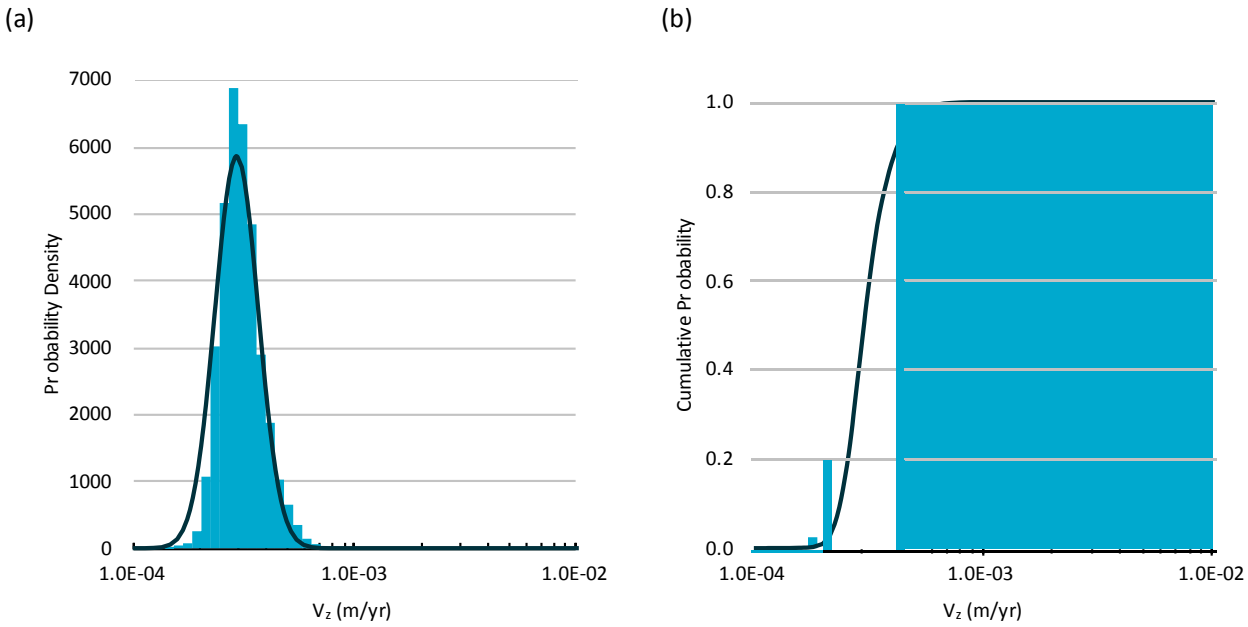


**Figure 4.4 Probability of vertical velocity of Evergreen Formation at Condabri MB9-H; (a) Probability density function and (b) cumulative density function**

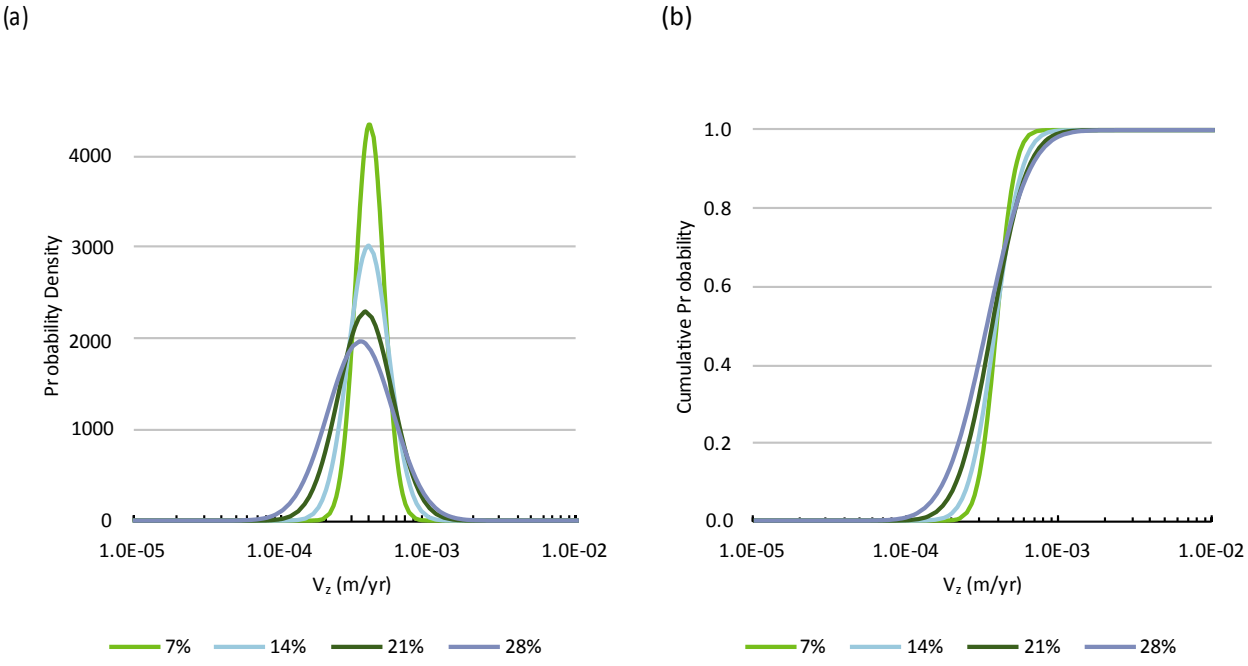


**Figure 4.5 Permeability probability and the dependency on uncertainty in helium measurements for the Evergreen Formation and lower Hutton Sandstone at Condabri MB9-H; (a) probability density functions and (b) cumulative probability functions**

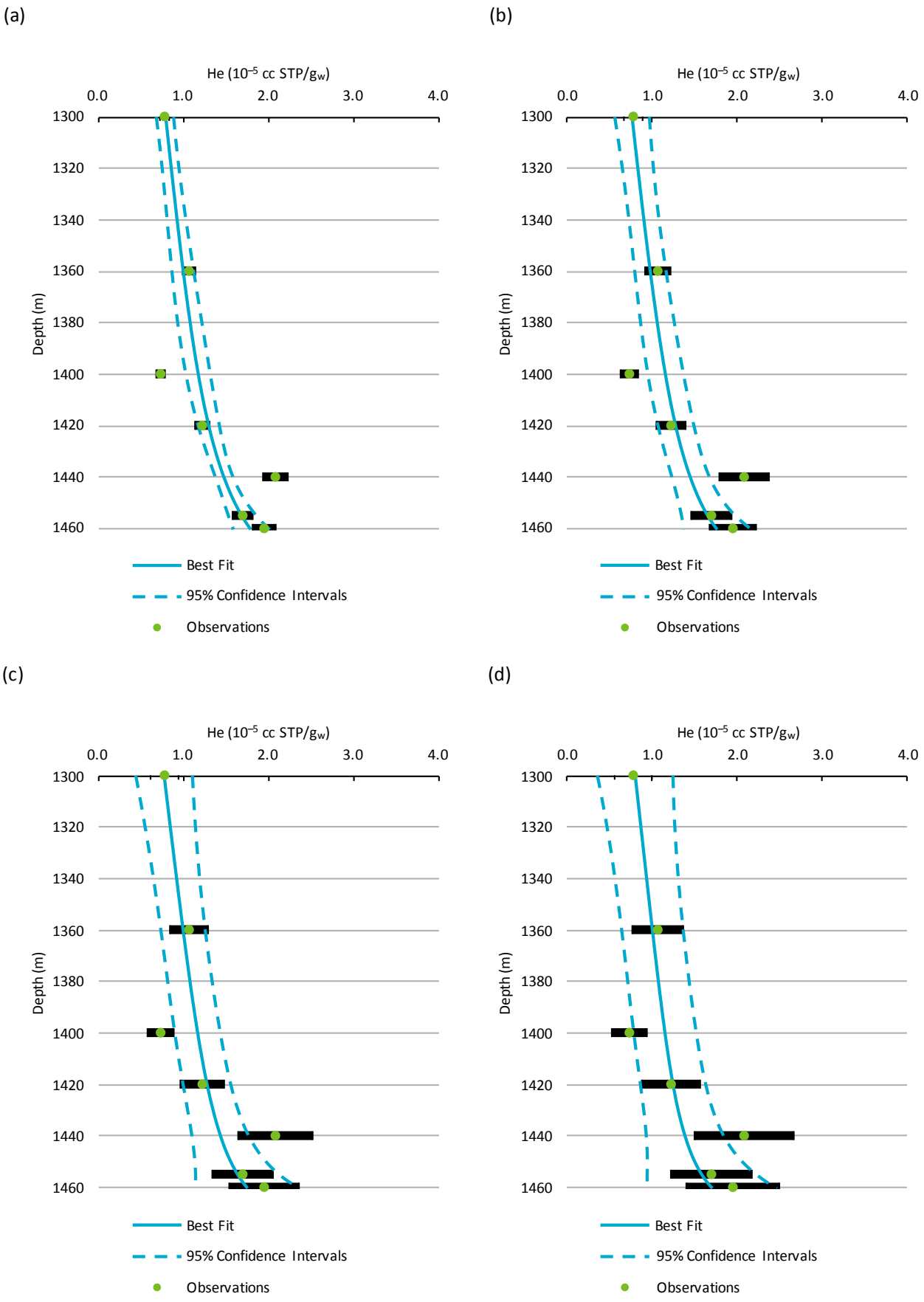


**Figure 4.6 Modelled helium distribution for the Evergreen Formation only at Condabri MB9-H – helium concentration uncertainties of (a) 7%, (b) 14%, (c) 21%, and (d) 28%**

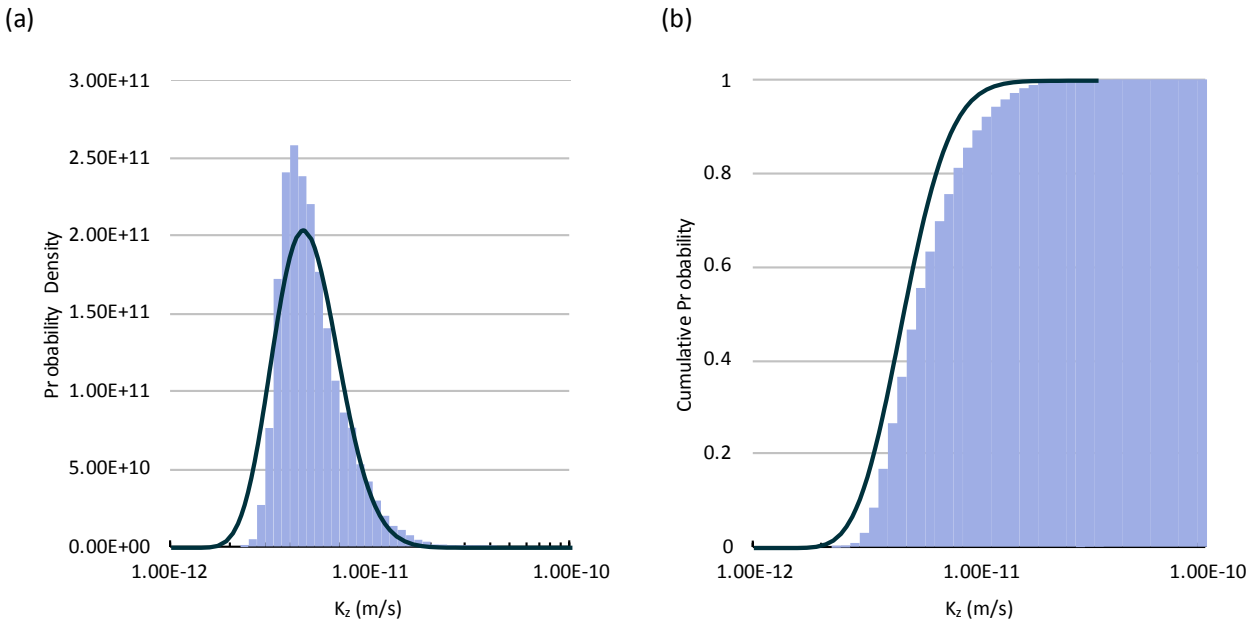


**Figure 4.7 Probability of hydraulic conductivity of Evergreen Formation at Condabri MB9-H; (a) Probability density function and (b) cumulative density function**

## Evergreen and lower Hutton

Monte Carlo simulations of one-dimensional helium transport across the gamma derived aquitard (Evergreen Formation and lower Hutton Sandstone) at Condabri MB9-H yield a PDF of velocity with a logarithmic normal distribution (Figure 4.8a). The mean vertical fluid velocity is $4.3\pm1.0\times10^{-4}$ m/year. The median is $4.2\times10^{-4}$ m/year and the mode is $4.0\times10^{-4}$ m/year. The cumulative probability (Figure 4.8b) indicates a 90% probability that the vertical velocity is less than $5.3\times10^{-4}$ m/s and a 99% probability that the velocity is less than $6.6\times10^{-4}$ m/year. Increasing the uncertainty by a factor of two and three causes the mean to increase by 6 and 13%, respectively. The standard deviations increased by 55 and 124%. The median values increased slightly at 3 and 6% and the mode decreased by 2 and 7%. The 90% probabilities increase by 9 and 19%, and 99% probabilities increase by 24 and 48%. Best-fit solutions and 95% probability is given in Figure 4.9.

The PDF for hydraulic conductivity has a logarithmic normal distribution with mean and standard deviation of $8.1\pm1.4\times10^{-12}$ m/s (Figure 4.10a). The median and mode are $8.0\times10^{-12}$, and $7.8\times10^{-12}$ m/s, respectively. The cumulative probability (Figure 4.10b) indicates a 90% probability that the vertical hydraulic conductivity is less than $9.6\times10^{-12}$ m/s and a 99% probability that the velocity is less than $1.2\times10^{-11}$ m/s.

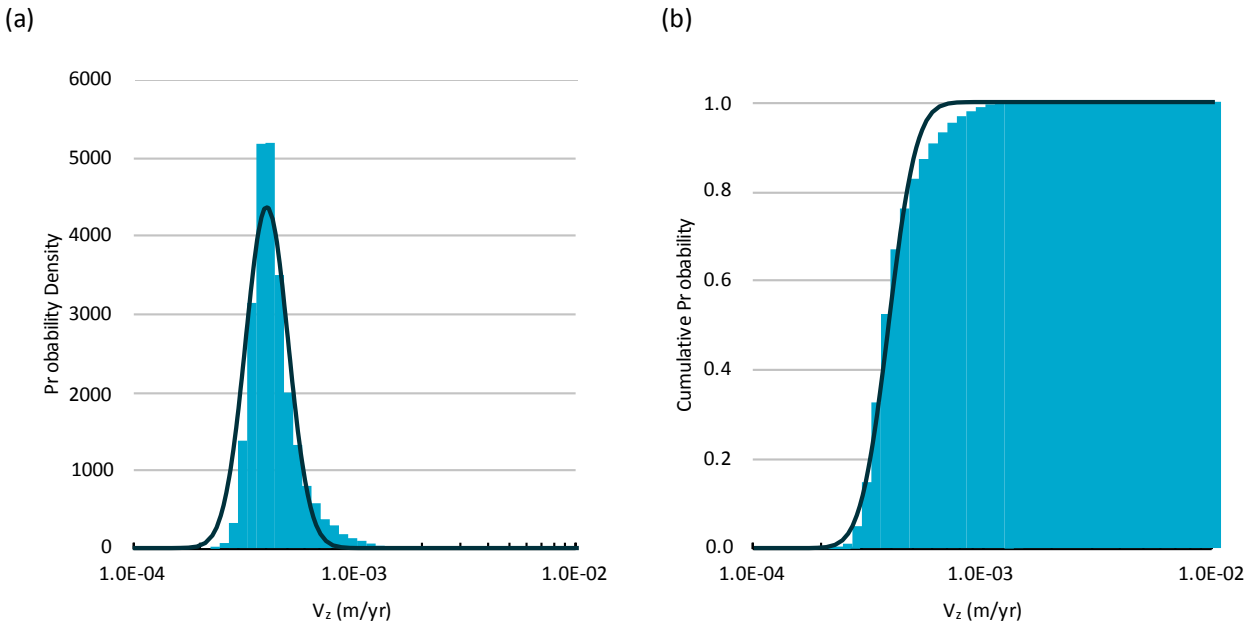


**Figure 4.8 Probability of vertical velocity of Evergreen Formation and the lower Hutton Sandstone at Condabri MB9-H; (a) Probability density function and (b) cumulative density function**

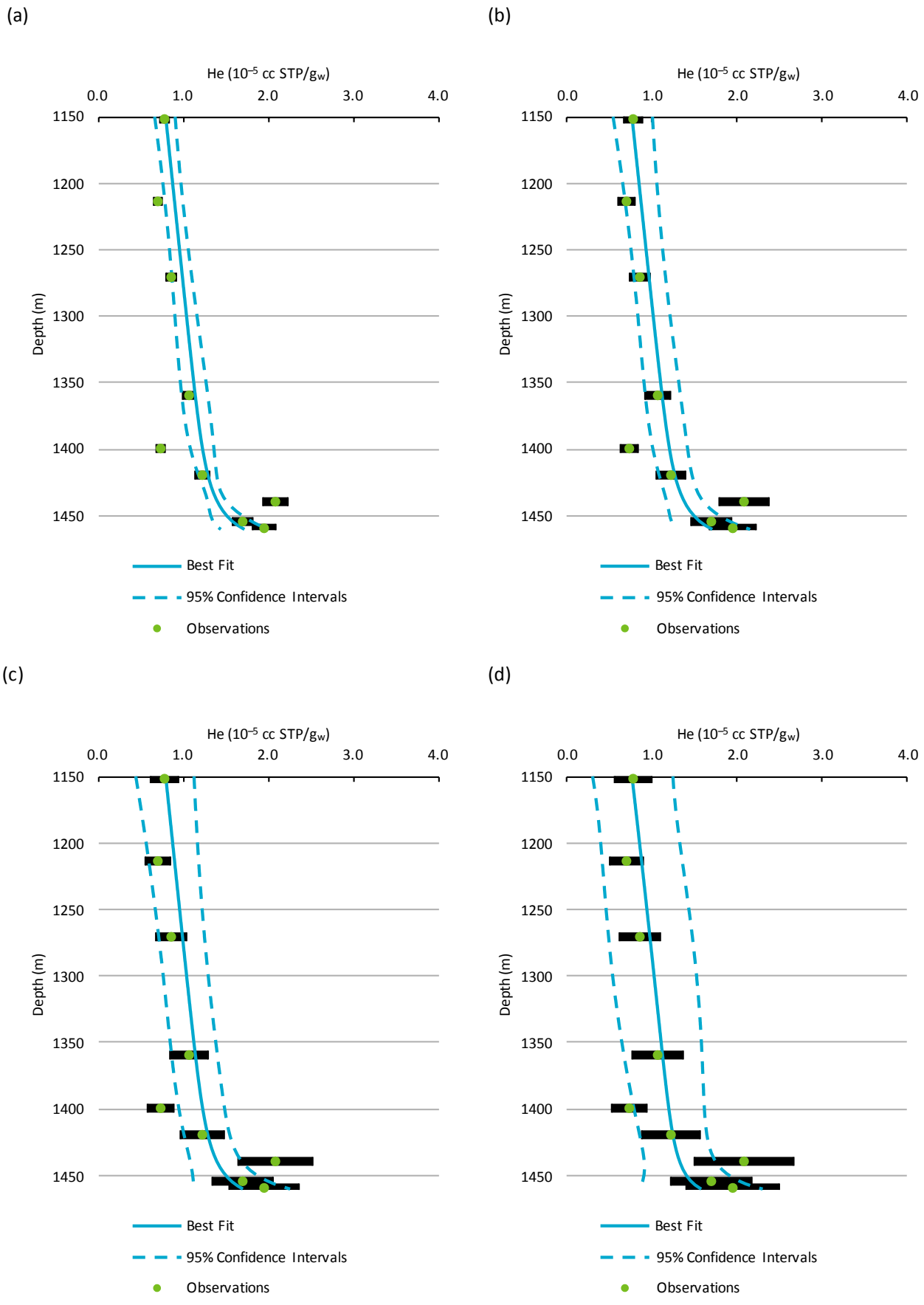


**Figure 4.9 Modelled helium distribution for the Evergreen Formation and lower Hutton Sandstone at Condabri MB9-H; helium concentration uncertainties of (a) 7%, (b) 14%, (c) 21%, and (d) 28%**

(a)

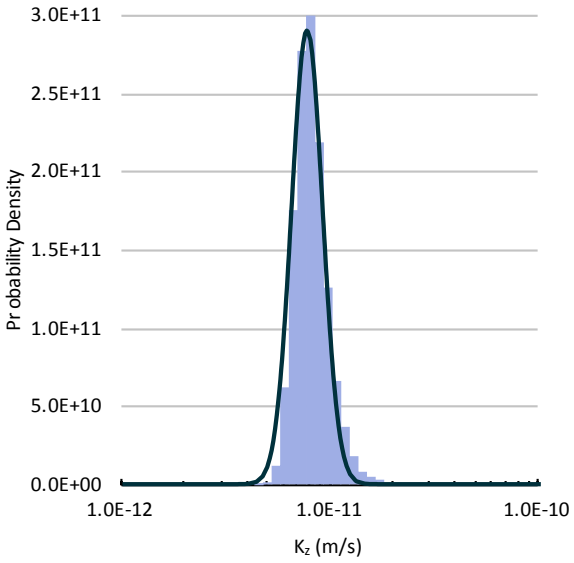


(b)

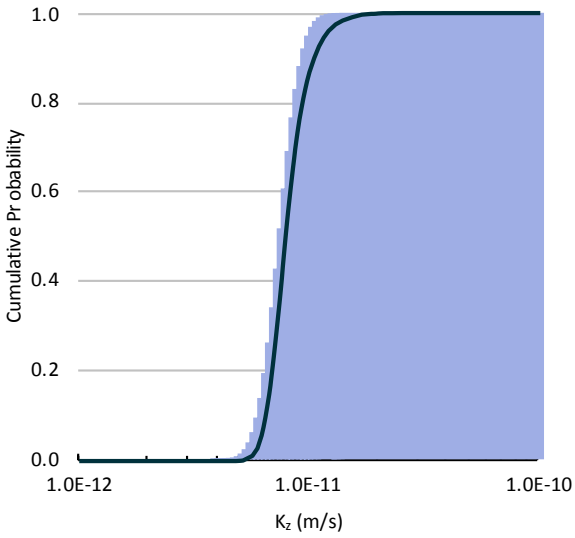


**Figure 4.10 Probability of hydraulic conductivity of Evergreen Formation and the lower Hutton Sandstone at Condabri MB9-H; (a) Probability density function and (b) cumulative density function**

### 4.5.2 CONDABRI EUROMBAH FORMATION

With only one boundary condition and two helium concentrations in the Eurombah Formation, it is currently not possible to create a constrained model of helium transport in this formation.

### 4.5.3 REEDY CREEK EVERGREEN FORMATION

While there are no clear trends in helium concentration across the Evergreen Formation at this site, an attempt was made to model the fluid velocity. The Monte Carlo simulation gives a bimodal distribution of velocities, with the major peak at $2\times10^{-10}$ m/year and a minor peak at $2\times10^{-3}$ m/year. The major peak is arbitrarily low and the resulting helium distribution is not representative of the observed values. The higher peak is representative of realistic velocities, but again the modelled helium distribution is not representative of the observed values (Figure 4.11). It is apparent that this simple transport model cannot be used to represent the fluid velocity and resulting helium distribution. This could be due to non-steady state conditions. A lack of additional information makes it very difficult if not impossible to define an initial condition for a transient model; therefore, unfortunately there is no clear solution to represent this data in a model.

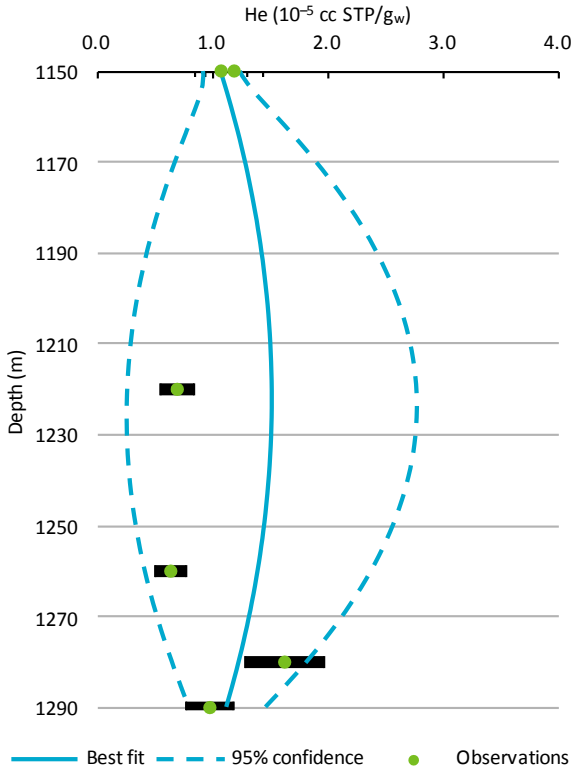


**Figure 4.11 Modelled helium distribution for the Evergreen Formation at Reedy Creek MB3-H**

### 4.5.4 REEDY CREEK WESTBOURNE FORMATION

Monte Carlo simulations of one-dimensional helium transport across the Westbourne Formation at Reedy Creek SC1 Wb yield a PDF of velocity with a bimodal logarithmic normal distribution (Figure 4.12a). By making calculations from maximum likelihood distribution, the mean vertical fluid velocity is $7.5\pm3.9\times10^{-4}$ m/year, the median is $6.6\times10^{-4}$ m/year and the mode is $5.2\times10^{-4}$ m/year. The maximum likelihood cumulative probability (Figure 4.4b) indicates a 90% probability that the vertical velocity is less than $1.3\times10^{-3}$ m/s and a 99% probability that the velocity is less than $2.1\times10^{-3}$ m/year. By relying on only the Monte Carlo probability distributions, the mode is slightly higher at $7.1\times10^{-4}$ m/year and the 90 and 99% probabilities decrease slightly to $1.1\times10^{-3}$ and $1.4\times10^{-3}$ m/year, respectively.

As mentioned above, the helium distribution here is very sensitive to the production rate. Using the helium production rate from the Hutton and Precipice sandstones, it was not possible to fit the observed helium distribution because the production rate was too low to achieve the 'bulge' seen in Figure 4.3b. By raising the helium release rate by a factor of 10, the observations could be fit by the model. Analysis of uranium and thorium concentrations in other sedimentary rocks indicates that shales, clays, silts and muds are only slightly enriched in U relative to the average upper crust. However, there are examples of very high U concentrations in sediments containing phoshorite, but without elemental or mineralogical analysis of these sediments, it is not possible to calculate the helium production rate and estimates are still necessary. Furthermore, helium release rates can exceed production rates by two orders of magnitude, however this has only been observed in shallow sediments (Solomon et al., 1996). The helium release rate could also be affected by the formation's porosity and tortuosity, both factors that strongly affect helium's effective diffusivity. Regardless of the cause, the results here indicate that vertical fluid velocities through the Westbourne Formation are quite low.

The PDF for hydraulic conductivity has a logarithmic normal distribution with mean and standard deviation of $7.9\pm3.6\times10^{-12}$ m/s (Figure 4.10a). The median and mode are $7.2\times10^{-12}$, and $6.0\times10^{-12}$ m/s, respectively. The cumulative probability (Figure 4.10b) indicates a 90% probability that the vertical hydraulic conductivity

is less than $1.25\times10^{-11}$ m/s and a 99% probability that the velocity is less than $1.95\times10^{-11}$ m/s. Increasing the uncertainty by a factor of two and three causes the mean to increase by 21 and 35%, respectively (Figure 4.5). The standard deviations increased by 84 and 164%, respectively. The median values increased slightly at 10 and 11% and the mode decreased by 10 and 25%, respectively. The 90% probabilities increase by 41 and 71%, and 99% probabilities increase by 71 and 161%, respectively.

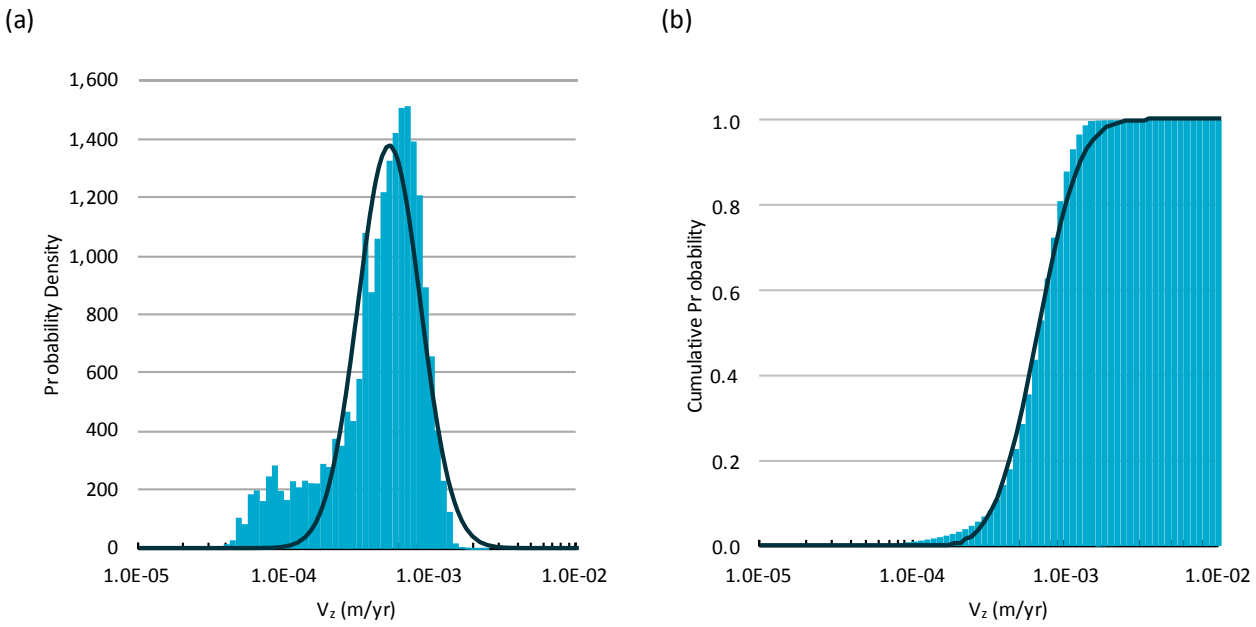


**Figure 4.12 Probability of vertical velocity of the Westbourne Formation at Reedy Creek SC1-Wb; (a) Probability density function and (b) cumulative density function**

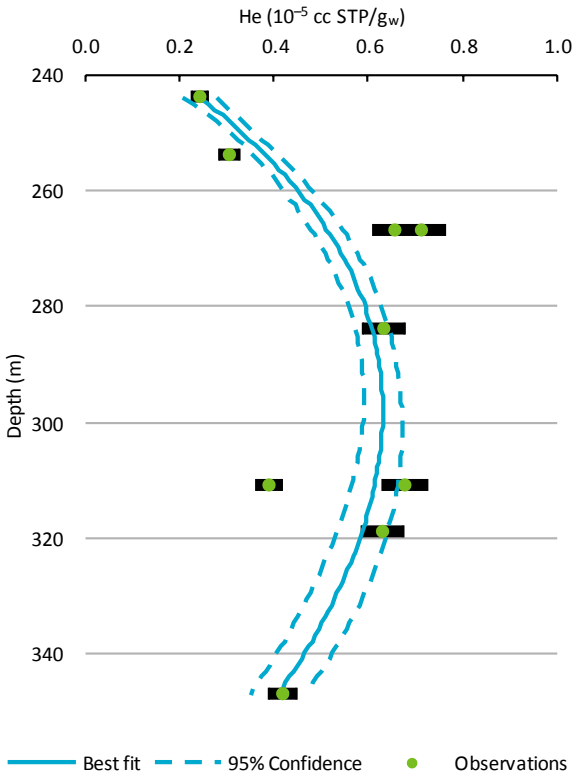


**Figure 4.13 Modelled and observed helium distributions for the Westbourne Formation at Reedy Creek SC1-Wb**

# 5 Discussion

## 5.1 Helium equilibrium

The degree of equilibrium can be assessed by comparing quartz-helium measurements to direct pore water measurements, or by comparing the results from different grain sizes. The former method is only possible at Reedy Creek where direct and quartz measurements are present in the same units. The later method is only possible from sample Reedy Creek MB3-H 1139 m and will be used below.

At Reedy Creek MB3-H 1139 m, the groundwater helium concentration calculated from the finer (54–75 µm) fraction was 10% greater than the coarser (75–150 µm) fraction. Considering the approximated 7% analytical uncertainty, these analyses are within two standard deviations of one another. Assuming that the difference in pore water helium concentrations is significant, the degree of equilibrium with the pore water can be calculated. The average helium concentration was calculated for both grain size fractions by assuming spherical grains (Crank, 1975) with a linear distribution of grain sizes (Figure 5.1 and Figure 5.2). With this model, the helium concentration in the fine and coarse fraction are 99.8 and 90.5% of the pore water concentration. This correction value is independent of the diffusivity and can be used as a correction factor to other measurements after correcting for temperature. This yields a pore water helium concentration of $1.19\times10^{-5}$ cc STP/g. The assumption of linear grain size distribution is reasonable without additional information.

To assess other distributions, it was assumed that the grain size fraction varied linearly with grain size, resulting in two scenarios where (1) the largest grain size was dominant and the smallest grain size was absent and (2) the smallest grain size was dominant and the largest grain size was absent. The latter case is likely the closest to reality for a fine-grained sample with a normal distribution of grain sizes, predominantly clays and silts. With dominantly coarse grains, the degree of equilibrium for the fine and coarse fractions are 99.8 and 90.1% (Figure 5.1 and Figure 5.2). With dominantly fine grains, the degree of equilibrium for the fine and coarse fractions are 98.9 and 89.1% (Figure 5.1 and Figure 5.2). The overall effect on the equilibrium pore water helium concentration is less than 1%, thus negating the need for precisely determining grain size distributions, unless the distributions have more extreme biases.

Regardless, future studies could quantitatively determine grain size distributions which could readily be applied to the model. It should be emphasized that this method assumes constant boundary conditions on each quartz grain. The model could be readily modified to include a linearly or exponentially changing boundary condition. However, external data would be needed to characterise the time-dependent boundary condition. This would likely include another tracer that could be used to determine historical hydraulic conditions.

Taking the age of the observed degree of equilibration, it can be broadly used as an indicator of when the system became steady state. From this assumption, it is possible to determine the degree of equilibrium for samples at other depths, and thus at different temperatures. Samples at 20, 40, 60, and 80 °C have degrees of equilibrium of 20.5, 64.7, 99.2, and 100%, respectively (Figure 5.3). As such, we can expect a high degree of equilibrium in the Evergreen Formation (~59 °C) and Precipice Sandstone (~62 °C), but much lower equilibrium in the Westbourne Formation (~28 °C).

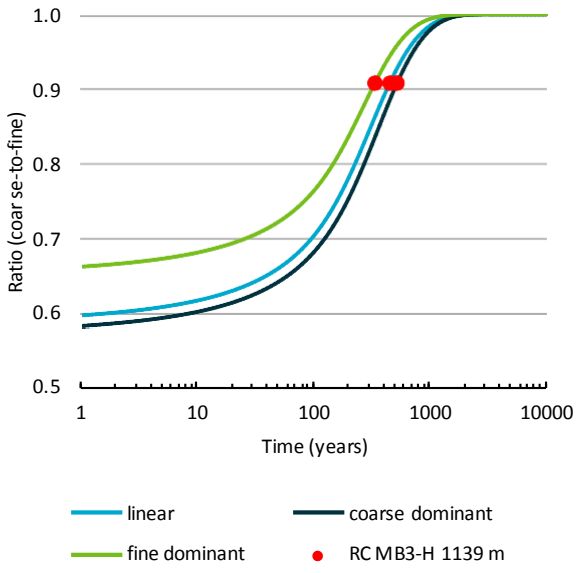


**Figure 5.1 Modelled ratio of coarse-to-fine helium concentrations for sample Reedy Creek MB3-H 1139 m as a function of time – see text for model parameters**

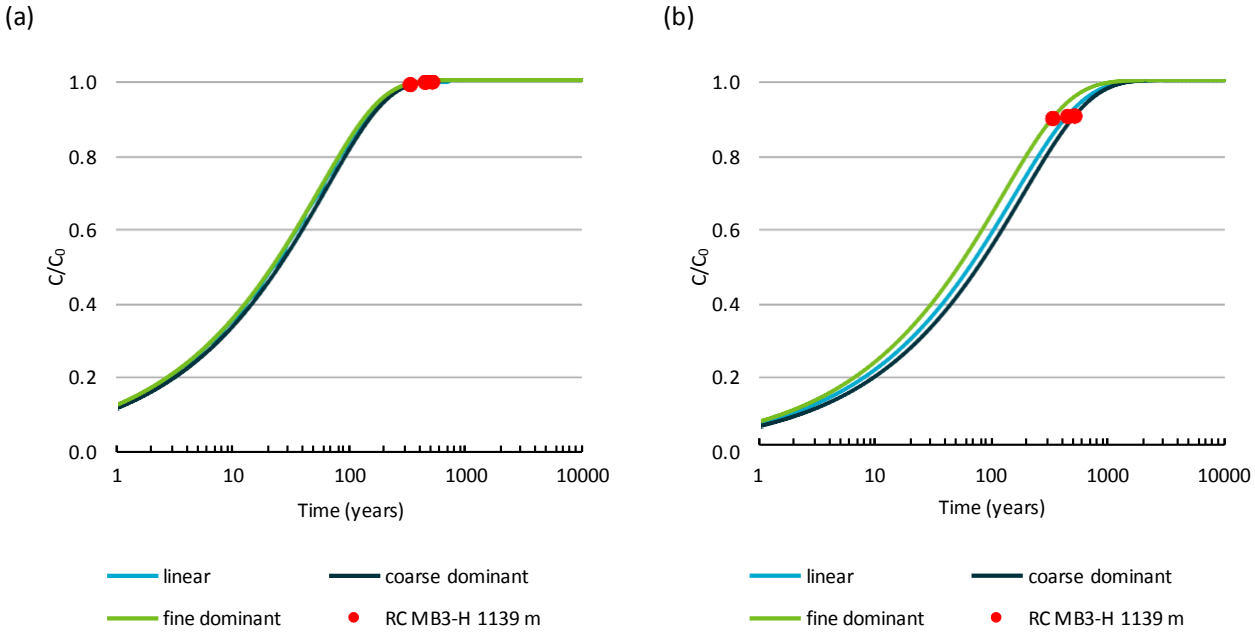


**Figure 5.2 Modelled normalized helium concentrations in (a) fine and (b) coarse fractions of sample Reedy Creek MB3-H 1139 m – see text for model parameters**

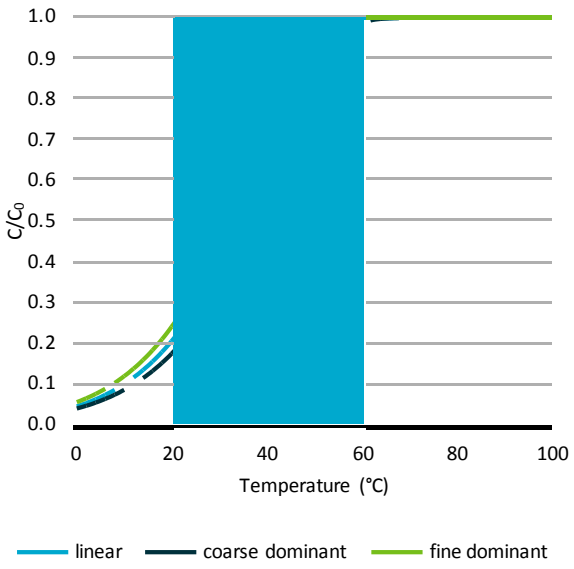


**Figure 5.3 Degree of equilibrium as a function of temperature – the shaded box represents temperatures in the Surat Basin**

## 5.2 Monte Carlo velocity modelling

Using the Monte Carlo approach to determine the fluid velocity appears to be an effective way of determining appropriate uncertainties. This method also shows a few points about the sensitivity of the model. When comparing the Evergreen-Hutton and Evergreen-only models, the fluid velocity and uncertainty are greater when the lower Hutton Formation is included in the model (Figure 4.4 and Figure 4.8). This increase in uncertainty can be attributed to having more data-points and thus more scatter in the data, but it also can be attributed to the sensitivity of the model at difference fluid velocities. Logically, at a very low fluid velocity, helium moves dominantly through diffusion. The resulting helium profile is a straight line between the boundary conditions. As fluid velocity decreases further, the helium profile remains unchanged as the effects of diffusion do not change. As the fluid velocity increases, this straight line becomes a curved line before becoming a vertical line with the value of the upgradient helium concentration. It is when the line is curved that there is the greatest sensitivity to the modelled fluid velocity. Using a generic aquitard with a thickness of 100 m and equal spacing between observations, artificial helium observations were created using varying fluid velocities. The helium distribution was then modelled using the Monte Carlo approach that has been used above. The distribution of these results is shown in Figure 5.4 and indicates that $1.6\times10^{-4}$ m/year has the greatest sensitivity at this scale. At fluid velocities below $6\times10^{-5}$ m/year, the uncertainty increases significantly. It should be noted that this ideal velocity will change as the model parameters change, including the diffusivity of helium, production rates, boundary concentrations and thickness of the model. This indicates that the diffusivity of the tracer should be matched to the target problem (other potential tracers of interest include stable isotopes of water and chloride). This can help ensure that the tracer profile is sensitive to the conditions present.

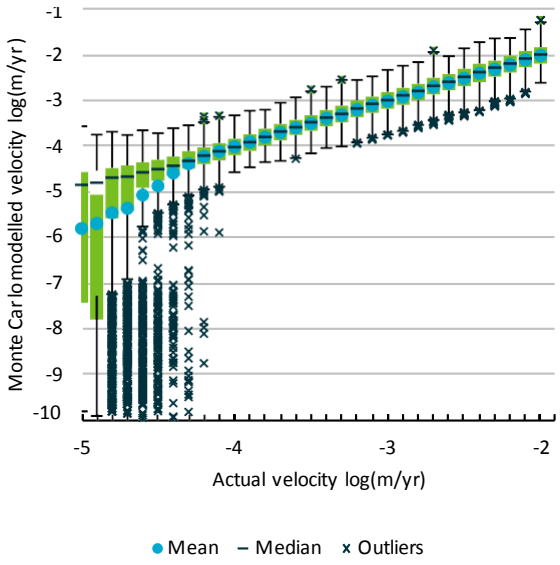


**Figure 5.4 Statistics of generic Monte Carlo simulations as a function of the actual velocity**

## 5.3 Modelled permeability

The vertical hydraulic conductivity of the Evergreen Formation at Condabri estimated here is within the range of previous vertical hydraulic conductivity estimates by laboratory triaxial tests and by centrifuge permeameter(Figure 5.5) (Australia Pacific LNG, 2013). This suggests the features present in the core-scale may be effective at preventing fluid flow at the formation-scale. Furthermore, this value agrees with the hydraulic conductivity values that have been used for previous modelling efforts (University of Southern Queensland, 2011). Even with increasing the uncertainty associated with helium measurements, the hydraulic conductivity does not reach values significantly greater when considering the multiple orders of magnitude that hydraulic conductivity can take on.

However, it should be stressed that this value may not be valid on a regional-scale. It is likely that this method has an averaging affect in the vertical direction, but with limited averaging horizontally. This is with the assumption that horizontal fluid flow and horizontal helium transport in the aquitard is negligible, but this has not been determined through modelling with appropriate vertical and horizontal hydraulic gradients.

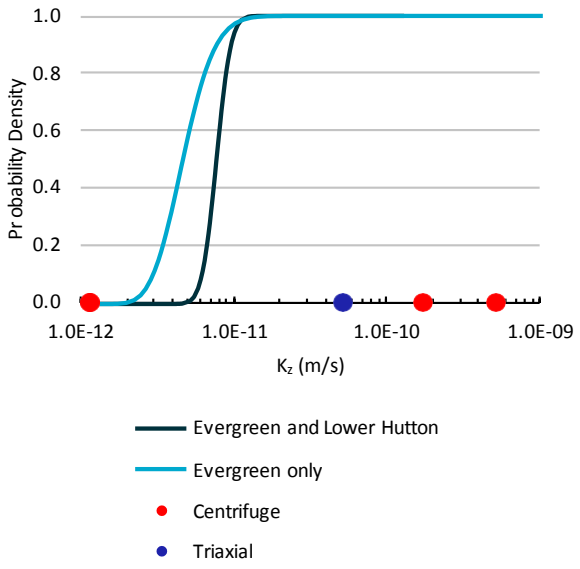


**Figure 5.5 Estimates of hydraulic conductivity for the Evergreen Formation at Condabri; centrifuge and triaxial estimates are from APLNG (2013)**

## 5.4 Limitations

### 5.4.1 VALIDITY OF STEADY STATE

The greatest limitation to using helium to constrain fluid transport through aquitards is the assumption of steady state conditions. Lacking an independent assessment of initial conditions and how boundary conditions change with time, the modelling of helium relies on the assumption of steady state. Because it takes millennia to produce large helium concentrations in groundwater, there is an assumption that the flow paths are adequately long, thus attenuate any temporal changes in fluid velocity and flow direction that could influence the helium concentrations. However, without multi-dimensional solute transport modelling and a constrained basin history, this assumption cannot be validated. In this study, the modelled fluid velocities and vertical hydraulic conductivities rely on this assumption and there was no assessment if the same helium profiles could be the result of changes in boundary conditions. Therefore, the fluid velocities and hydraulic conductivities presented here must be regarded as best estimates based on the available data – stressing that alternative models may explain the observed data.

Future studies may be able to constrain this assumption. However, as mentioned, it would require a robust understanding of the basin history, which would need to be properly represented in a groundwater model.

### 5.4.2 VALIDITY OF ONE-DIMENSIONAL TRANSPORT

As briefly mentioned before, the use of a one-dimensional model in a three-dimensional system has limitations. Any lateral heterogeneities caused by faults, fractures, or changes in lithology cannot be assessed in a rigorous manner. For example, if a sample site is located immediately adjacent to a fracture, the helium concentrations within the fracture could be significantly different than the helium concentration in the unfractured portion of the formation – diffusion of helium toward or away from the fracture could perturb the distribution of helium at the sample site. Furthermore, if fluids with a high concentration of helium are introduced across the vertical profile by means of lateral flow, this high concentration could be misinterpreted as a fluid transport mechanism that is not characteristic of the rest of the vertical profile.

The role of these lateral heterogeneities and their effects on helium concentrations may be further constrained by measuring helium profiles in several nearby cored wells, giving the potential to constrain a two- or three-dimensional transport model.

### 5.4.3 HETEROGENEITY OF HELIUM PRODUCTION

In the one-dimensional modelling described above, the helium production rate was modelled to vary with a given standard deviation, but the spatial distribution of helium production was always assumed constant for each simulation. As advection and/or diffusive flux of helium increase, the effect of the helium production rate is diminished. However, in scenarios where the production rate is significant, the spatial heterogeneity can become a significant modelling factor. To assess the effect of heterogeneous helium production, a simple one-dimensional model was created in MODFLOW. The hydraulic boundary conditions were set to create zero vertical gradient. In each of the 32 layers, the helium production rate was randomized with a normal distribution about a mean value. The boundary helium concentrations were fixed and ten scenarios were modelled and the helium distribution at steady state was recorded.

In Figure 5.6a, it is apparent that helium concentrations are affected the greatest in the centre of the model domain; in this scenario, concentrations at the centre of the model have a standard deviation of 1.6%. When comparing the homogenous and heterogeneous cases, Figure 5.6b shows that the average production rate does not accurately estimate the total helium present in the model. This is because high or low production rates near the boundaries of the model have little effect on the helium concentrations in the centre of the model. To better assess the correlation of total helium to the production rate, a weighting factor was applied to the production rates where boundary production rates have less weight than production rates in the centre of the model domain. A linear distribution of weighting factors appears to be the most appropriate Figure 5.7. Figure 5.7a indicates that high helium production rates have a reduced effect on modelled helium distributions. For example, if the weighted helium production rate increases by 10%, the extra amount of helium in the model domain only increases by approximately 2%. It should be noted that this value is expected to change with different aquitard thicknesses. For example, a very thin aquitard would not be affected by heterogeneous production rates because diffusive fluxes increase as the formation thickness decreases.

In the diffusion-dominated modelling performed here, the effects of heterogeneous helium distributions seem to significantly affect the modelled helium distributions. However, this effect is expected to diminish when advection plays a greater role in helium transport. As such, the heterogeneous distribution of helium production rates are not expected to greatly affect the permeabilities calculated above, especially for the Evergreen Formation at Condabri where the production rate has only slight effects on the best fit velocity (see Appendix C ). However, this result suggests that knowledge of the spatial distribution of production rates will be advantageous in future studies.

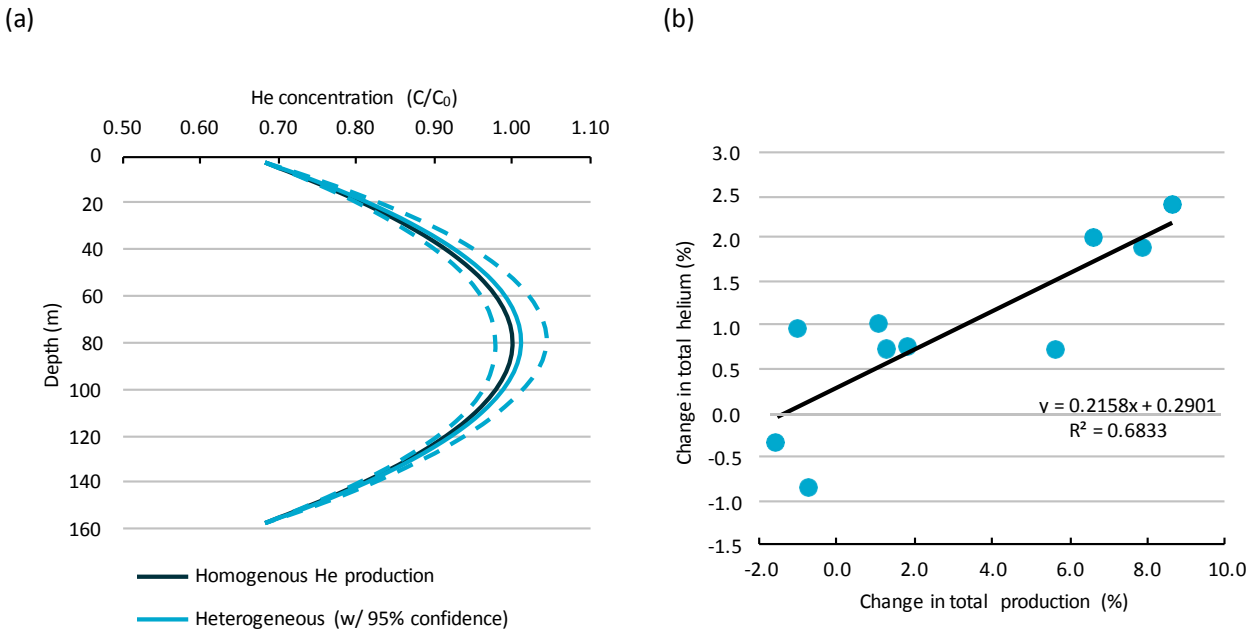


**Figure 5.6 Modelled helium distributions showing the effects of heterogeneous helium distributions; (a) Helium distributions with depth for homogenous and heterogeneous helium production rates and (b) total helium concentrations as a function of the average production rate**

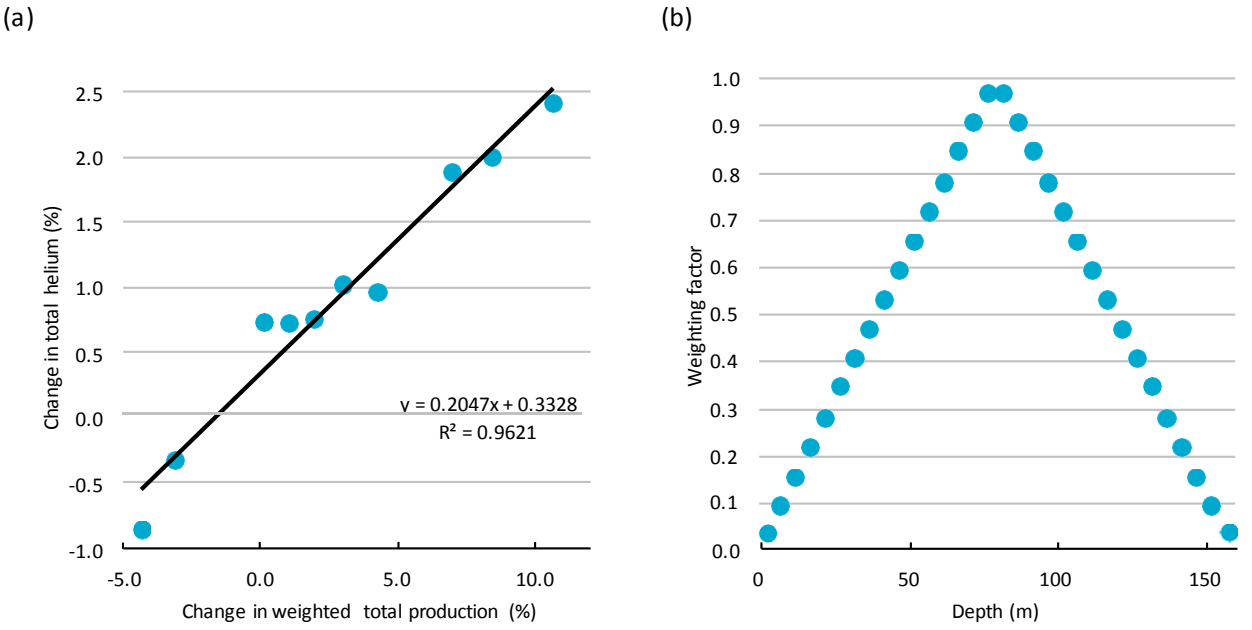


**Figure 5.7 The effects of spatially weighting the helium production rates; (a) The total helium concentrations as a function of the weighted total production rate, (b) the linear weighting factor as a function of depth**

### 5.4.4 QUARTZ-HELIUM EQUILIBRIUM

This aspect of the method is by far the greatest remaining hurdle. It is surprisingly difficult to find quartz samples that appear to have complete equilibrium of helium in relation to the pore water. Correction factors may help with this issue, but overall there is a limitation when the initial state of disequilibrium is unknown. This may indicate that non-steady state conditions are more prevalent and deep aquifers are more dynamic than expected. The best path to solving this issue is likely to be a very thorough analysis of grain shape, physical and chemical impurities, and how these factors affect the diffusion and retention of helium. Without solving this issue, the quartz-helium method will always have some doubt surrounding the

validity of calculated pore water helium concentrations. However, this study has shown that it is possible to find logical trends at the formation-scale, which in turn is very helpful in constraining vertical fluid fluxes that are ultimately used to calibrate groundwater flow models and become tools to determine vertical leakage.

# 6 Conclusions

The quartz-helium method has the potential to constrain the fluid velocity and bulk permeability of low permeability formations in a manner unmatched by more conventional methods. At the Condabri site, the Evergreen Formation appears to be a competent seal with very slight vertical leakage on the order of $3.1\times10^{-4}$ m/year. Equilibrium of helium between pore water in quartz appears to be the limiting process, but a fair agreement is seen between quartz measurements and direct measurements in the Precipice Sandstone. The deeper formations within the Surat Basin appear to be ideal targets for using this method. However, it is noted that the aquitards separating the more shallow aquifers and coal measures are where the biggest questions lie as these aquitards will play the greatest role in cross formational flow. Monte Carlo simulations appear effective in constraining the permeability range, especially when one-dimensional transport with steady state conditions can be assumed. Future refinements to the method could include greater quantification of quartz-pore water helium equilibrium. Overall, this method shows promise for quantifying formation-scale flow in complex systems.

# Appendix A Core list

### Apx Table A.1 Cores provided by Origin Energy

| WELL | DEPTH TOP ( m) | DEPTH BOTTOM (m) | FORMATION | APPROX MASS* (g) |
|---|---|---|---|---|
| **TALINGA MB3-H** | 670.00 | 670.06 | Hutton Sst | 375.2 |
| | 690.16 | 690.22 | Hutton Sst | 551.5 |
| | 709.65 | 709.71 | Hutton Sst | 382.1 |
| | 730.10 | 730.17 | Hutton Sst | 450.0 |
| | 750.35 | 750.40 | Hutton Sst | 365.4 |
| | 770.85 | 770.91 | Hutton Sst | 424.7 |
| | 790.84 | 790.90 | Hutton Sst | 390.8 |
| | 809.86 | 809.93 | Hutton Sst | 470.9 |
| | 830.77 | 830.83 | Hutton Sst | 350.0 |
| | 852.00 | 852.05 | Hutton Sst | 354.1 |
| | 870.46 | 870.50 | Hutton Sst | 284.8 |
| | 892.77 | 892.83 | Hutton Sst | 356.9 |
| | 912.37 | 912.45 | Hutton Sst | 547.3 |
| | 932.73 | 932.79 | Hutton Sst | 351.9 |
| | 952.36 | 952.43 | Hutton Sst | 457.0 |
| **REEDY CREEK MB3-H** | 841.93 | 841.99 | Hutton Sst | 357.1 |
| | 860.26 | 860.31 | Hutton Sst | 327.0 |
| | 880.86 | 880.92 | Hutton Sst | 354.4 |
| | 900.83 | 900.93 | Hutton Sst | 611.8 |
| | 918.50 | 918.55 | Hutton Sst | 263.6 |
| | 941.43 | 941.48 | Hutton Sst | 361.7 |
| | 960.21 | 960.26 | Hutton Sst | 387.1 |
| | 980.62 | 980.69 | Hutton Sst | 381.3 |
| | 1002.91 | 1003.00 | Hutton Sst | 413.0 |
| | 1020.54 | 1020.60 | Hutton Sst | 422.3 |
| | 1040.64 | 1040.69 | Hutton Sst | 387.8 |
| | 1060.78 | 1060.87 | Hutton Sst | 698.7 |
| | 1080.93 | 1081.00 | Hutton Sst | 477.3 |
| | 1100.45 | 1100.49 | Hutton Sst | 249.6 |

| WELL | DEPTH TOP ( m) | DEPTH BOTTOM (m) | FORMATION | APPROX MASS* (g) |
|---|---|---|---|---|
| | 1120.87 | 1120.92 | Hutton Sst | 361.0 |
| | 1139.81 | 1139.87 | Hutton Sst | 414.0 |
| | 1160.20 | 1160.28 | Evergreen Fm | 569.9 |
| | 1181.25 | 1181.32 | Evergreen Fm | 477.2 |
| | 1200.35 | 1200.40 | Evergreen Fm | 374.4 |
| | 1220.56 | 1220.62 | Evergreen Fm | 427.9 |
| | 1242.36 | 1242.41 | Evergreen Fm | 343.5 |
| | 1260.27 | 1260.33 | Evergreen Fm | 428.7 |
| | 1280.28 | 1280.35 | Evergreen Fm | 502.9 |
| | 1298.43 | 1298.50 | Precipice Sst | 479.9 |
| | 1320.47 | 1320.52 | Precipice Sst | 416.2 |
| | 1337.65 | 1337.70 | Precipice BSF | 359.2 |
| **TALINGA MB5-G** | 53.43 | 53.49 | Gubberamunda Sst | 242.1 |
| | 73.05 | 73.10 | Gubberamunda Sst | 297.5 |
| | 79.10 | 79.15 | Gubberamunda Sst | 264.3 |
| **TALINGA SCI-WB** | 98.30 | 98.35 | Westbourne Fm | 304.1 |
| | 118.34 | 118.39 | Westbourne Fm | 296.8 |
| | 142.56 | 142.62 | Westbourne Fm | 382.1 |
| | 159.25 | 159.30 | Westbourne Fm | 363.4 |
| | 179.03 | 179.08 | Westbourne Fm | 348.7 |
| | 198.92 | 198.97 | Westbourne Fm | 344.3 |
| **TALINGA MB7-S** | 208.96 | 209.02 | Springbok Fm | 433.5 |
| | 219.59 | 219.65 | Springbok Fm | 436.8 |
| **REEDY CREEK SCI-WB** | 244.20 | 244.26 | Westbourne Fm | 430.3 |
| | 251.29 | 251.33 | Westbourne Fm | |
| | 253.5 | 253.55 | Westbourne Fm | |
| | 254.81 | 254.86 | Westbourne Fm | |
| | 257.71 | 257.75 | Westbourne Fm | |
| | 259.54 | 259.61 | Westbourne Fm | |
| | 267.29 | 267.34 | Westbourne Fm | 290.9 |
| | 284.35 | 285.41 | Westbourne Fm | 343.9 |
| | 300.76 | 300.81 | Westbourne Fm | |
| | 304.26 | 304.31 | Westbourne Fm | 290.7 |

| WELL | DEPTH TOP ( m) | DEPTH BOTTOM (m) | FORMATION | APPROX MASS* (g) |
|---|---|---|---|---|
| | 304.5 | 304.55 | Westbourne Fm | |
| | 308.73 | 308.79 | Westbourne Fm | |
| | 311.81 | 311.85 | Westbourne Fm | |
| | 319.4 | 319.46 | Westbourne Fm | |
| | 324.23 | 324.29 | Westbourne Fm | 375.2 |
| | 344.57 | 344.62 | Westbourne Fm | 233.7 |
| | 347.90 | 347.95 | Westbourne Fm | 298.7 |
| **RCMB2-S** | 382.25 | 382.30 | Springbok Fm | 287.3 |
| | 389.90 | 389.95 | Springbok Fm | 284.7 |
| | 406.00 | 406.05 | Springbok Fm | 279.0 |
| **CONDABRI MB9-H** | 1024.42 | 1024.50 | Eurombah Fm | 406.2 |
| | 1040.95 | 1041.01 | Eurombah Fm | 433.8 |
| | 1061.57 | 1061.62 | Eurombah Fm | 323.3 |
| | 1072.22 | 1072.28 | Hutton Sst | 448.6 |
| | 1090.49 | 1090.55 | Hutton Sst | 337.4 |
| | 1110.22 | 1110.27 | Hutton Sst | 362.8 |
| | 1131.2 | 1131.25 | Hutton Sst | 365.6 |
| | 1152.2 | 1152.27 | Hutton Sst | 417.3 |
| | 1171.7 | 1171.74 | Hutton Sst | 310.3 |
| | 1191.11 | 1191.16 | Hutton Sst | 327.8 |
| | 1214.37 | 1214.42 | Hutton Sst | 369.1 |
| | 1229.53 | 1229.58 | Hutton Sst | 360.3 |
| | 1251.09 | 1251.16 | Hutton Sst | 434.0 |
| | 1271.43 | 1271.49 | Hutton Sst | 493.4 |
| | 1289.68 | 1289.74 | Hutton Sst | 372.1 |
| | 1303.34 | 1303.39 | Evergreen Fm | 245.2 |
| | 1320.16 | 1320.22 | Evergreen Fm | 431.2 |
| | 1340.82 | 1340.88 | Evergreen Fm | 414.8 |
| | 1360.95 | 1361.00 | Evergreen Fm | 347.0 |
| | 1380.92 | 1380.97 | Evergreen Fm | 338.8 |
| | 1400.39 | 1400.44 | Evergreen Fm | 400.7 |
| | 1420.72 | 1420.76 | Evergreen Fm | 346.3 |
| | 1440.69 | 1440.73 | Evergreen Fm | 559.3 |
| | 1455.19 | 1455.24 | Evergreen Fm | 325.3 |

| WELL | DEPTH TOP ( m) | DEPTH BOTTOM (m) | FORMATION | APPROX MASS* (g) |
|---|---|---|---|---|
| | 1459.79 | 1459.84 | Precipice Sst | 382.7 |
| | 1481.46 | 1481.50 | Precipice Sst | 434.6 |
| | 1500.72 | 1500.77 | Precipice BSF | 365.9 |
| **Strathblane WB1-P**** | 324 | 325 | N/A | |
| | 338 | 339 | N/A | 190.0 |
| | 348 | 349 | N/A | |
| | 358 | 359 | N/A | |

*Weights include plastic bag tha t contains sample (~3g); **Cuttings only

# Appendix B Gamma logs

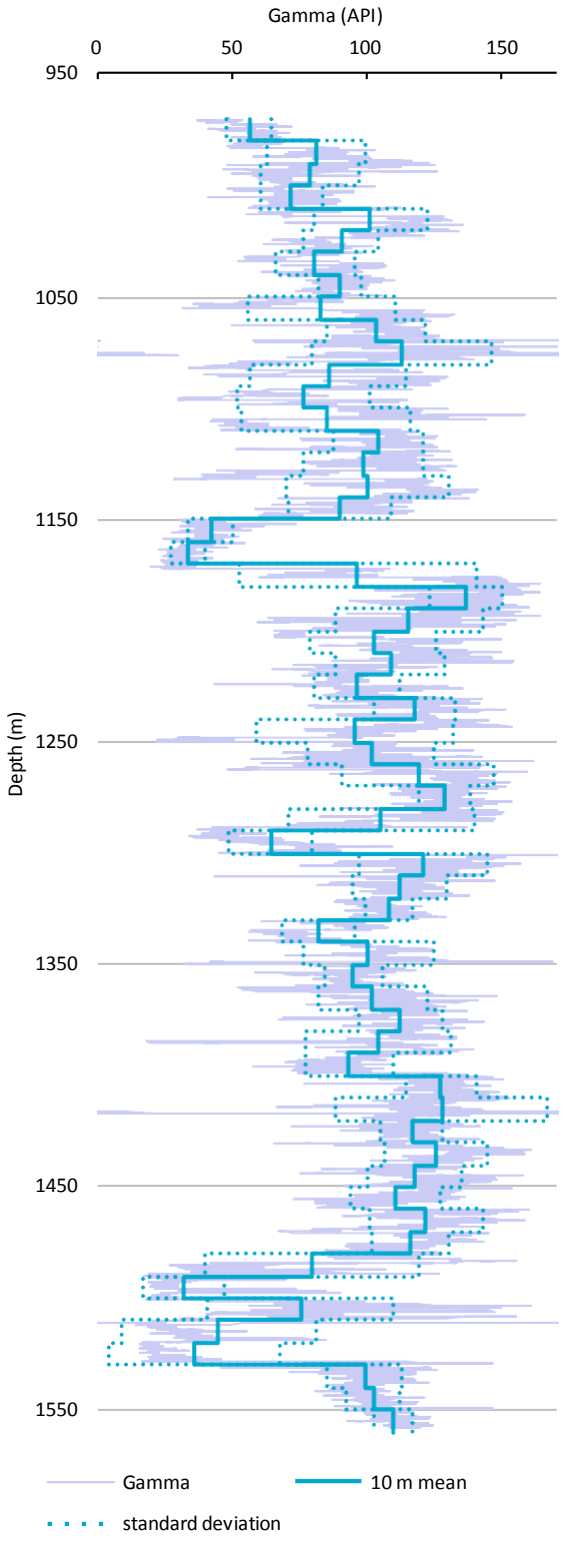


Apx Figure B.1 Gamma log for Condabri MB9-H

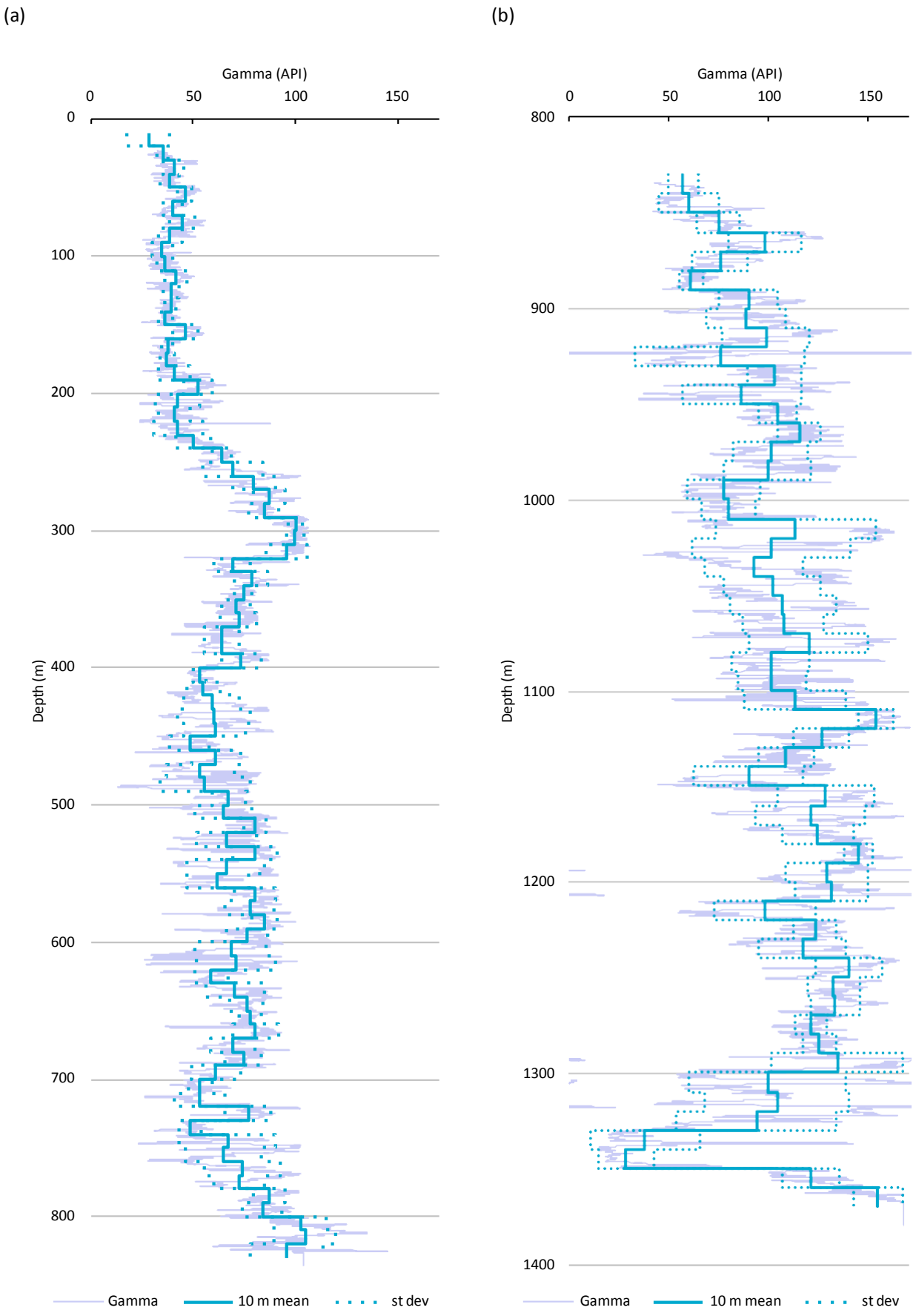


**Apx Figure B.2 Gamma log for Reedy Creek MB3-H; (a) <835 m and (b) >835 m**

# Appendix C Model parameters and outputs

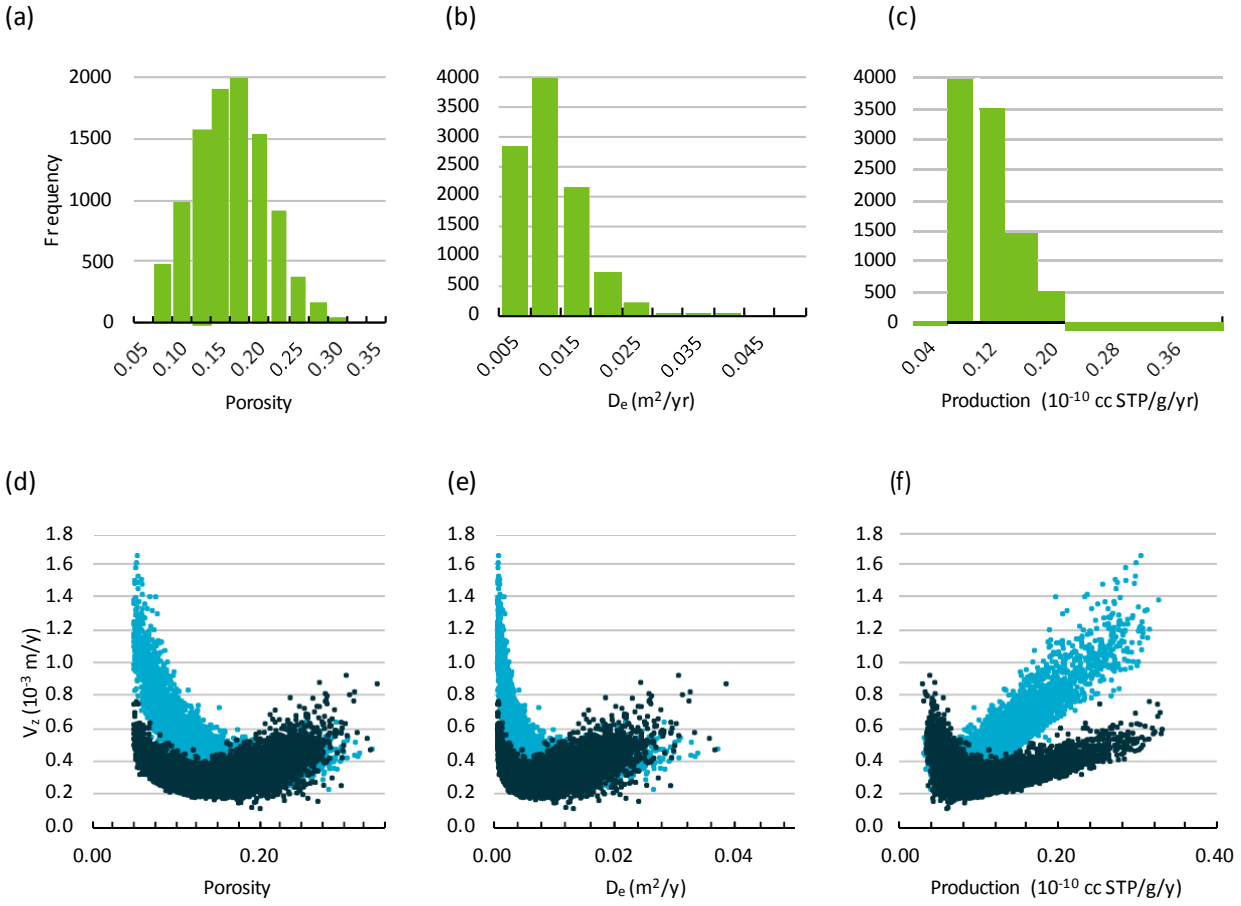


**Apx Figure C.1 Distribution of input parameters (a, b, c) used to model the Evergreen and lower Hutton Formation and trends with best fit vertical velocity (d, e, f). In d, e, and f: black = Evergreen Formation only, Blue = Evergreen Formation and lower Hutton Sandstone.**

# References


Australia Pacific LNG (2011) Condabri MB9-H well completion report.

Australia Pacific LNG (2013) 2013 groundwater assessment.

Ballentine CJ and Burnard PG (2002) Production, release and transport of noble gases in the continental crust. In: Porcelli D, Ballentine CJ and Wieler R (eds) Reviews in Mineralogy and Geochemistry. Mineralogical Society of America, Geochemical Society, Washington, DC, 481-538.

Barrell J (1914) The strength of the earth's crust. Journal of Geology 22(1), 28-48.

Crank J (1975) The Mathematics of Diffusion. Clarendon, Oxford.

Exon NF (1976) Geology of the Surat Basin in Queensland. Bureau of Mineral Resources, Australia.

Gannibal MA (2012) Equilibrium helium partitioning in the rock-water system: New prospects for dating ancient groundwater. Geochemistry International 50(1), 8-17.

Gardner WP and Solomon DK (2009) An advanced passive diffusion sampler for the determination of dissolved gas concentrations. Water Resources Research 45, W06423.

Jähne B, Heinz G and Dietrich W (1987) Measurement of the diffusion coefficients of sparingly soluble gases in water. Journal of Geophysical Research 92, 10767-10776.

Kellett JR, Radke BM, Ransley TR, Bell JG and Stewart GA (2012) Chapter 5: Hydrogeological framework. In: Smerdon BD and Ransley TR (eds) Water resource assessment for the Surat region. A report to the Australian Government from the CSIRO Great Artesian Basin Water Resource Assessment. CSIRO Water for a Healthy Country Flagship, Australia.

Kowalczuk PB and Drzymala J (2012) Surface flotation of particles on liquids. Principles and applications. Colloids and Surfaces a-Physicochemical and Engineering Aspects 393, 81-85. DOI: 10.1016/j.colsurfa.2011.11.004.

Lehmann BE, Waber HN, Tolstikhin I, Kamensky I, Gannibal M and Kalashnikov E (2003) Helium in solubility equilibrium with quartz and porefluids in rocks; a new approach in hydrology. Geophysical Research Letters 30(3), 4.

Mazurek M, Alt-Epping P, Bath A, Gimmi T, Waber HN, Buschaert S, De Canniere P, De Craen M, Gautschi A, Savoye S, Vinsot A, Wemeare I and Wouters L (2011) Natural tracer profiles across argillaceous formations. Applied Geochemistry 173(1-4), 219-240.

Osenbrück K, Lippmann J and Sonntag C (1998) Dating very old pore waters in impermeable rocks by noble gas isotopes. Geochimica et Cosmochimica Acta 62(18), 3041-3045.

Rosenblum S (1958) Magnetic susceptibilities of minerals in the Frantz isodynamic magnetic separator. The American Mineralogist 43, 170-173.

Shuster DL and Farley KA (2005) Diffusion kinetics of proton-induced 21Ne, 3He, 4He in quartz. Geochimica et Cosmochimica Acta 69, 2349-2359.

Smerdon BD, Ransley TR, Radke BM and Kellett JR (2012) Water resource assessment for the Great Artesian Basin. A report to the Australian Government from the CSIRO Great Artesian Basin Water Resource Assessment. CSIRO Water for a Healthy Country Flagship, Australia.

Smith SD (2012) Helium equilibrium between pore water and quartz: application to determine caprock permeability. University of Utah.

Smith SP and Kennedy BM (1983) The solubility of noble-gases in water and NaCl brine. Geochimica Et Cosmochimica Acta 47(3), 503-515. DOI: 10.1016/0016-7037(83)90273-9.

Solomon DK, Hunt A and Poreda RJ (1996) Source of radiogenic helium 4 in shallow aquifers: Implications for dating young groundwater. Water Resources Research 32(6), 1805-1813.

Trull TW, Kurz MD and Jenkins WJ (1991) Diffusion of cosmogenic 3He in olivine and quartz; implications for surface exposure dating. Earth and Planetary Science Letters 103(1-4), 241-256.

University of Southern Queensland (2011) Preliminary Assessment of Cumulative Drawdown Impacts in the Surat Basin Associated with the Coal Seam Gas Industry. University of Southern Queensland.

Weiss RF (1971) Solubility of helium and neon in water and seawater. Journal of Chemical & Engineering Data 16(2), 235-241. DOI: 10.1021/je60049a019.

CONTACT US

**t** 1300 363 400
+61 3 9545 2176
**e** enquiries@csiro.au
**w** www.csiro.au

YOUR CSIRO

Australia is founding its future on science and innovation. Its national science agency, CSIRO, is a powerhouse of ideas, technologies and skills for building prosperity, growth, health and sustainability. It serves governments, industries, business and communities across the nation.